Master's thesis

NTNU
Norwegian University of Science and Technology
Faculty of Medicine and Health Sciences
Department of Clinical and Molecular Medicine

Mathilde Homstad

In vitro effects of the AMP-activated protein kinase agonist metformin on murine osteocytes MLO-Y4

Master's thesis in Molecular Medicine
Supervisor: Astrid Kamilla Stunes
May 2020

NTNU
Norwegian University of Science and Technology

In vitro effects of the AMP-activated protein kinase agonist metformin on murine osteocytes MLO-Y4

Mathilde Homstad

Master of Science in Molecular Medicine

Trondheim, May 2020

Principal supervisor: Astrid Kamilla Stunes

Co-supervisor: Mats Peder Mosti

Norwegian University of Science and Technology

Faculty of Medicine and Health Sciences

Department of Clinical and Molecular Medicine

NTNU
Norwegian University of
Science and Technology

Abstract

Osteoporosis is a common skeletal disease associated with increased risk of fragility fractures, characterized by impaired bone quality and low bone mass, and it is a growing concern due to an aging population. Weight-bearing exercise is known to be a countermeasure against osteoporosis and it is known to activate AMP-activated protein kinase (AMPK). Likewise, metformin is an AMPK activator, and previous research on bone cells have revealed beneficial effects on bone physiology. Few studies have previously studied the effect of metformin in osteocytes. Therefore, this study aimed to investigate the effect of metformin on osteocyte survival and osteocyte markers related to the response of mechanical load, to investigate whether metformin can mimic mechanical load in osteocytes in vitro.

The murine osteocyte-like cell line MLO-Y4 was used as a model for osteocytes, and the cells were stimulated with 100 µM, 500 µM and 2000 µM metformin and compared to controls in all experiments. LDH activity assay and MTT proliferation assay were used to study toxicity and proliferation, respectively. qPCR was used for examination of gene expression of *RANKL*, *OPG*, *Ptgs2*, *Sost*, *Wnt1* and *Wnt3a*, and a monoclonal ELISA assay was used to study protein expression of PGE_2. Furthermore, an ELISA cell death detection kit was used to examine the effect of metformin on apoptosis following ionizing radiation.

Metformin does not increase LDH activity in MLO-Y4 osteocytes in the given concentrations, but appear to decrease cytotoxic damage to the cells exposed to a dose of 100 µM. Metformin inhibits proliferation of MLO-Y4 cells in high doses (500 and 2000 µM). mRNA expression of *OPG* and *RANKL* are not significantly regulated by metformin, but it appears that the RANKL/OPG ratio is decreased with higher doses of metformin. The mRNA expression of the mechanosensitive ion channel Piezo1 is significantly upregulated dose-dependently after 24 hours of metformin stimulation. Metformin does not significantly regulate mRNA expression of osteocyte markers *Sost*, *Ptgs2*, *Wnt3a* and *Wnt1* after 24, 48 and 72 hours, all genes related to the mechanical load response. Protein secretion of mechanical-load inducible PGE_2 is not upregulated by metformin. Following 5 Gy ionizing radiation of MLO-Y4 cells, metformin appears to prevent the apoptotic response to the radiation in a dose-dependent matter, but this needs to be confirmed with further experiments. In conclusion, metformin is not a direct mimetic of exercise and mechanical load, but some responses are similar. It will also be of future interest to investigate whether there is an additive effect of combining mechanical load and metformin stimulation in osteocytes in vitro.

Sammendrag

Osteoporose er en skjelettsykdom som gir økt risiko for beinbrudd. Sykdommen karakteriseres av nedsatt beinkvalitet og lav beinmasse, og er en økende bekymring grunnet en økt aldrende befolkning. Styrketrening er vist å forebygge osteoporose, i tillegg til å aktivere AMPK. Metformin er også en AMPK-aktivator, og tidligere forskning på beinceller har vist gunstige effekter på beinmetabolismen. Få studier har tidligere studert effekten av metformin hos osteocytter. Derfor ønsket vi gjennom denne studien å studere hvordan metformin påvirker viabiliteten til osteocytter, og å analysere osteocyttmarkører knyttet opp mot responsen vi ser ved trening. Gjennom disse eksperimentene ønsket vi å se om metformin kan etterligne effekten av mekanisk belastning i osteocytter in vitro. Den murine osteocytt-cellelinjen MLO-Y4 ble brukt som en modell for osteocytter, og cellene ble stimulert med 100-, 500-, og 2000 µM metformin, og sammenlignet med kontroll i alle eksperimentene. LDH aktivitets-analyse og MTT proliferasjonsanalyse ble brukt for å studere henholdsvis toksisitet og proliferasjon. qPCR ble brukt for å analysere genuttrykket av *RANKL, OPG, Ptgs2, Sost, Wnt1* og *Wnt3a*, mens et monoklonalt ELISA kit ble brukt for å studere proteinsekresjonen av PGE_2. Videre ble et ELISA kit for deteksjon av celledød brukt for å undersøke effekten metformin har på apoptose i osteocytter etter ioniserende stråling.

Resultatene viser at metformin ikke øker LDH aktiviteten i MLO-Y4 celler i gitte konsentrasjoner, men ser ut til å redusere cytotoksisk skade på cellene utsatt for en dose på 100 µM. Metformin hemmer proliferasjon av MLO-Y4 osteocytter i høye doser (500 µM og 2000 µM). mRNA-uttrykket av *OPG* og *RANKL* reguleres ikke signifikant av metformin, men det ser ut til at RANKL/OPG ratioen reduseres med økende doser. Vi fant at mRNA-uttrykket av den mekanosensitive ionekanalen Piezo1 doseavhengig oppreguleres signifikant etter 24 timer med metformin. Metformin gir ingen signifikant regulering av mRNA-nivåene for *Sost*, *Ptgs2*, *Wnt3a* og *Wnt1* etter 24, 48 og 72 timer, der alle genene er kjent for å reguleres av trening og mekanisk belastning. Proteinsekresjonen av PGE_2 er kjent for å øke etter mekanisk belastning, men våre resultater viser ingen oppregulering etter stimulering med metformin. Etter en dose på 5 Gy med ioniserende stråling viser våre foreløpige resultater at metformin kan ha en dose-avhengig preventiv effekt på den økende apoptosen forårsaket av strålingen hos MLO-Y4 osteocytter, men dette må bekreftes med videre eksperimenter. For å konkludere, så ser det ikke ut til at metformin direkte etterligner effekten av trening, men at noen responser er like. I fremtidig forskning vil det være av interesse å undersøke om metformin og trening kombinert kan gi en additiv effekt på osteocytter in vitro.

Acknowledgements

This master thesis was carried out as a part of the master program in Molecular Medicine at the Norwegian University of Science and Technology (NTNU). The work for the thesis was performed at the Department of Clinical and Molecular Medicine in the Endocrinology and Bone metabolism research group.

Many thanks to my main supervisor Astrid Kamilla Stunes for all your support and for the theoretical and practical guidance throughout the year. Thank you for sharing all your knowledge with me and for the continuous feedback during the period of writing. I could never have finished my thesis without all your help. I would also like to thank medical physicist and Associate Professor Anne Beate Langeland Marthinsen and Associate Professor Katherine Røe Redalen for help with the radiation, and my co-supervisor Mats Peder Mosti for useful input and guidance. Furthermore, I would also like to thank a fellow student, Vincent Jongen, for all his help with the project in the lab and for useful discussions regarding our projects.

Finally, I would like to thank my family and my boyfriend Brynjar for their love and support throughout the year, and especially for motivating me during the tough times in the writing process.

Trondheim, May 2020

Mathilde Homstad

Table of Contents

List of figures

List of tables

Abbreviations

AChE	Acetylcholine esterase
AICAR	5-Aminoimidazole-4-carboxamide ribonucleotide
ALP	Alkaline phosphatase
AMPK	AMP activated protein kinase
BMD	Bone mineral density
BMP	Bone morphogenetic protein
BMPC	Bone marrow progenitor cells
BMU	Basic multicellular unit
BSP II	Bone sialoprotein 2
cDNA	Complementary deoxyribonucleic acid
COX-2	Cyclooxygenase-2
CS	Calf serum
DMP-1	Dentin matrix protein-1
ELISA	Enzyme-linked immunosorbent assay
FCS	Fetal calf serum
FGF-23	Fibroblast growth factor 23
GAPDH	Glyceraldehyde 3-phosphate dehydrogenase
Gy	Gray
HRP	Horseradish peroxidase
HMGB1	High motility group box 1
IGF-1	Insulin-like growth factor 1
LCS	Lacuno-canalicular system
LDH	Lactate dehydrogenase
LRP5/6	Low density lipoprotein-related protein 5 and 6
M-CSF	Macrophage-colony stimulating factor
MEM-α	Minimum essential medium alpha
MLO-Y4	Murine Long Bone Osteocyte Y4
MSC	Mesenchymal stem cell
MTT	3-(4,5-dimethylthiazol-2-yl)-2,5-diphenyl tetrazolium bromide
NO	Nitric oxide
OCN	Osteocalcin
OPG	Osteoprotegerin

Osx	Osterix
PBS	Phosphate-buffered saline
PG	Prostaglandin
PGE_2	Prostaglandin E_2
PHEX	Phosphate regulating endopeptidase homolog X-linked
PPARγ	Peroxisome proliferator-activated receptor gamma
PTH	Parathyroid hormone
qPCR	Quantitative polymerase chain reaction
RANKL	Receptor activator of nuclear factor kappa B ligand
ROS	Reactive oxygen species
RT	Radiation therapy
Runx2	Runt related transcription factor 2
SD	Standard deviation
SEM	Standard error of the mean
T2D	Type 2 diabetes
VEGF	Vascular endothelial growth factor

1. Introduction

1.1 Bone tissue

Bone is a mineralized type of connective tissue with a cellular component comprised by four main cell types: osteoclasts, osteoblasts, osteocytes and bone lining cells (1). Traditionally, bone has been considered a structural organ, important for locomotion and for providing mechanical protection and support for internal organs. It is also a reservoir for minerals, particularly calcium and phosphate and it harbors the bone marrow where blood cells are created (2, 3). Morphologically, bone can be divided into two histological types: cortical (compact) bone and cancellous (trabecular/spongy) bone (4). Cortical bone comprises up to 80% of total bone mass, mostly located in the diaphysis of long bones and the outer part of all skeletal structures (5). Cancellous bone has a porous web-like structure composed of trabeculae with a pore space filled with bone marrow and fat and is principally found in the axial skeleton and the epiphysis of long bones (6, 7). The surface-to-volume ratio is larger in cancellous bone, which results in a higher rate of bone remodeling and thus makes cancellous bone important in osteoporotic processes (7, 8). The extracellular matrix of bone contains an organic phase and an inorganic phase. The organic component consists mainly of type 1 collagen and other non-collagenous proteins that contribute to the tensile strength of bone, while the inorganic component is mainly calcium phosphate crystals and is important for bone strength and stiffness (4, 8).

1.2 Bone cells

1.2.1 Osteoclasts

Osteoclasts are terminally differentiated multinucleated cells derived from monocytes/ macrophages of the hematopoietic stem cell lineage. Their main function is to resorb bone through the degradation of organic and inorganic matrix (2, 9). Osteoclastogenesis is critically dependent on the cytokines macrophage-colony stimulating factor (M-CSF) and receptor activator of nuclear factor-kappa B ligand (RANKL). M-CSF is secreted by osteoprogenitor mesenchymal cells and osteoblasts, and binds to receptors on the osteoclast to promote proliferation and survival of osteoclast precursors. RANKL is secreted by osteoblasts, osteocytes and stromal cells and binds to its receptor RANK on osteoclast precursors to stimulate osteoclast differentiation, resorption and survival (2, 10). When the gene encoding RANKL is disrupted in mice, the animals display severe osteopetrosis and lack osteoclasts completely due to the inability to support osteoclastogenesis, demonstrating the importance of RANKL (11). In contrast, RANKL overexpression causes a severe osteoporotic phenotype (12). Osteoprotegerin (OPG) is a glycoprotein secreted by several cells, including osteoblasts

and osteocytes and act as a soluble decoy receptor for RANKL. OPG is a target of β-catenin and binding of OPG antagonizes the effects of RANKL, inhibiting osteoclastogenesis (3, 13).

When bone resorption is signaled by other cells, hematopoietic precursors are recruited to sites of bone remodeling and undergo osteoclastogenesis. Mature osteoclasts polarize through reorganization of the cytoskeleton when attaching to the bone surface to create a sealing zone and a ruffled border, which is in contact with the mineralized bone matrix (2). In the ruffled border, an H^+/ATPase proton pump acidifies the resorption lacuna to a pH of 4.5, which dissolves the inorganic hydroxyapatite crystals. A bicarbonate/chloride exchanger maintains intracellular pH. Cathepsin K, which is a lysosomal protease, and metalloproteinases degrade the organic collagen components. The degraded products are endocytosed by the osteoclast and transcytosed to the basolateral surface of the osteoclast where it is released (2, 9).

1.2.2 Osteoblasts

Osteoblasts are bone forming cells located along the bone surface originating from the mesenchymal stem cell lineage (MSC), which also gives rise to adipocytes, chondrocytes and muscle cells. Osteoblasts constitute about 4-6 % of all bone cells and their main functions are bone matrix protein secretion, bone mineralization and they give rise to osteocytes (2, 14).

The master regulator of early osteoblast differentiation is Runt-related transcription factor 2 (Runx2) which, in addition to osterix (Osx), drives the MSC progenitors into osteochondro progenitors (14). Runx2 upregulates the expression of osteoblastogenesis marker genes, including genes for type 1 collagen, alkaline phosphatase (ALP) and osteocalcin (OCN) (2, 15). The two transcription factors are crucial for osteoblastic differentiation and are activated by members of the Wnt family and bone morphogenetic proteins (BMPs) (Figure 1.1) (2, 16). Following the differentiation phase, the precursors that are now considered preosteoblasts, proliferate and show ALP activity. The preosteoblasts increase their expression of Osx, which is upregulated downstream of Runx2, and start to secrete bone matrix proteins, such as OCN, bone sialoprotein 2 (BSP II) and type 1 collagen (2, 17). At this transitional stage, the cells undergo morphological changes, acquiring a large and cuboidal form (14).

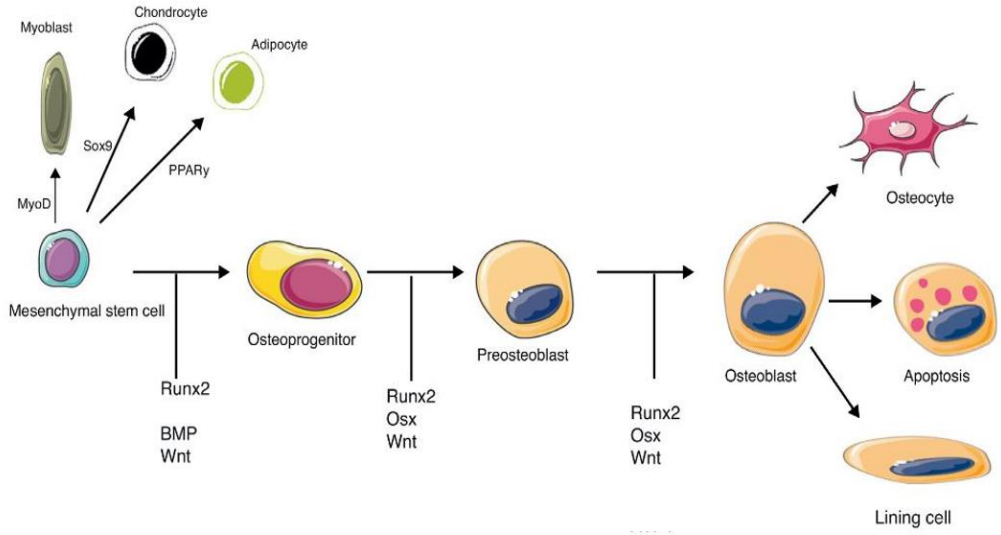

Figure 1.1: Osteoblast differentiation*. The molecular control of osteoblast differentiation from mesenchymal stem cells and the fate of mature osteoblasts. The figure is modified from Arboleya and Castañeda (18).*

Mature osteoblasts show high ALP activity and synthesize high amounts of bone matrix proteins, which turns into bone matrix at the bone surface. There are two principal steps of bone matrix synthesis: deposition of organic matrix and mineralization phase (14). First, mature osteoblasts make the organic matrix (osteoid) through secretion of type 1 collagen and noncollagenous proteins, such as OCN, BSP II, osteonectin, osteopontin and proteoglycans. Thereafter, mineralization is initiated, in which calcium ions and phosphate ions nucleate and then hydroxylate to form inorganic hydroxyapatite $Ca_{10}(PO_4)_6(OH)_2$ (14, 18). The crystals of hydroxyapatite are then released into extracellular space to fill gaps between collagen fibrils to comprise the inorganic matrix of bone (2). Upon completion of bone formation, osteoblasts face three destinies: undergo apoptosis, get trapped in the osteoid to become osteocytes or become bone lining cells (19). The latter is a quiescent flat cell which function to cover the bone surface to avoid contract between the osteoclast and bone matrix during resting phases of bone remodeling (14).

1.2.3 Osteocytes

Osteocytes are terminally differentiated bone cells and comprise up to 90-95% of the cells in the adult bone tissue (20, 21). They descend from osteoblasts and are the cells embedded in the bone matrix. Previously, the osteocyte has not received much attention and was considered a passive cell, but they are now known to play important functions in bone (22). One of its main functions is to act as mechanosensory cells, translating mechanical signals to chemical signals to regulate the process of bone remodeling (23, 24).

1.2.3.1 Differentiation and morphology

In the transition phase where osteoblasts become osteocytes, major morphological changes occur in the future osteocyte. The cuboidal osteoblasts specialized for matrix secretion start to extend cytoplasmic processes towards neighboring osteocytes and the mineralizing front (25, 26). The protein E11/gp38 is an important protein implicated in the early formation of dendritic processes in the embedding osteocyte (22). Zhang et.al demonstrated that dendrite formation in the osteocyte-like cell line MLO-Y4 was blocked after inhibition of E11, and that fluid flow shear stress increases length and number of dendrites (27). Thus, E11 appear to be critical for dendrite elongation and osteocyte function and viability. Other morphological changes during osteocytogenesis include cell body size reduction, and decrease of the number of organelles due to reduced protein synthesis (14).

At the mature stage of osteocytogenesis, osteoblast markers (BSPII, type 1 collagen and ALP) are downregulated and osteocyte markers are upregulated (Figure 1.2A) (2). Induction of *SOST* is an indicator of a mature osteocyte phenotype (28). Osteocyte markers include E11, phosphate regulating endopeptidase homolog X-linked (PHEX), matrix extracellular phosphoglycoprotein (MEPE), dentin matrix protein-1 (DMP-1), sclerostin and FGF-23 among others. FGF-23 is a hormone secreted predominantly by osteocytes and has endocrine functions. The hormone regulates phosphate metabolism in the kidneys through inhibition of phosphate reabsorption (3). FGF-23 levels are regulated by PHEX, MEPE and DMP-1, and is important in phosphate homeostasis and bone mineralization. When the osteoid is completely mineralized, the stellate shaped osteocyte become trapped in bone matrix, buried for its remaining life (25, 26).

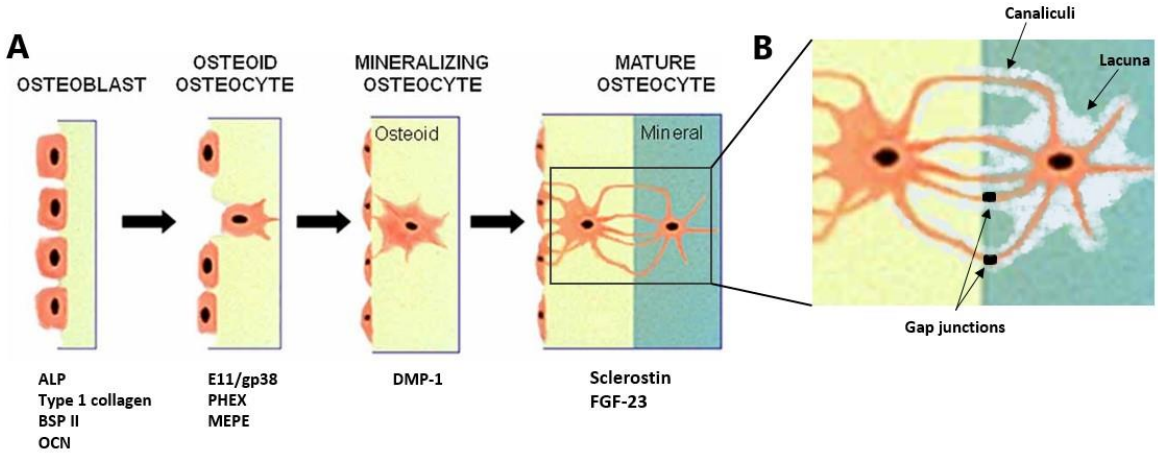

***Figure 1.2: The embedding osteocyte**. **A)** Differentiation of the osteocyte from the mature osteoblast and expression of markers during differentiation. **B)** The osteocyte is located in the lacuna and is connected to its neighbors through gap junctions. The dendrites are surrounded by channels called canaliculi. The figure is modified from Bonewald (22).*

1.2.3.2 Organization of the osteocyte network and mechanosensation

Mature osteocytes are localized within spaces known as lacunae, surrounded by mineralized bone matrix (2). The cytoplasmic processes reach for the processes of other osteocytes through tiny channels known as canaliculi (Figure 1.2B). Together, these structures form the lacuno-canalicular system (LCS) (25). This system allows the flow of interstitial fluid, which carries signaling factors and nutrients to and from osteocytes, and enables osteocyte communication through gap junctions and release of soluble mediators (29).

The osteocytes are recognized as mechanosensory cells. The flow of fluid through canaliculi enables osteocytes to sense mechanical load, and translate these mechanical signals into biochemical signals that affect bone remodeling processes (14). The molecular mechanisms in which osteocyte are able to sense mechanical load still remain somewhat unclear. It has been suggested that cell surface proteins such as focal adhesion proteins, cytoskeletal proteins, integrins and primary cilia are able to sense mechanical load (2, 22). Several studies have proposed that calcium channels are involved in osteocyte mechanosensation through the influx of Ca^{2+} shortly after exposure to mechanical stimuli that generates membrane deformation (30-32). In osteocytes, several mechanosensitive ion channels are expressed. Piezo1 is a mechanosensitive calcium ion channel and its expression in osteocytes is highly upregulated following fluid flow shear stress. Administration of a Piezo1 agonist led to increased bone mass and acted as a mimetic to mechanical load (33). Loss of Piezo1 resulted in a blunted response to mechanical loading, but it was not completely abolished. Additionally, this loss led to increased bone resorption through increased RANKL expression. These results suggest that osteocytes can sense and respond to mechanical signals through activation of Piezo1, but indicate that there are other additional mechanosensors (33).

1.2.3.3 Osteocyte communication and mechanotransduction

Osteocyte communication occur within the osteocyte network, but also with osteoblasts, bone lining cells and the vasculature. Osteocytes use a direct form of communication through gap junctions, which is cytoplasmic channels between two adjacent cells, made by connexin proteins (25). The connexin Cx43 is highly expressed in bone and has gained attention for its role in prevention of osteocyte apoptosis and response to mechanical loading (34, 35). Small molecules can pass through gap junctions, such as ions, low weight signaling molecules and nucleotides (25). Paracrine signaling is another form of communication, where small molecules are delivered over a short distance.

In response to mechanical load, for example fluid flow shear stress, osteocytes secrete bone anabolic nitric oxide (NO), ATP and prostaglandins (PGs). NO is an inhibitor of bone resorption and promoter of bone formation and is produced by NO synthase in both osteocytes and osteoblasts (22). Prostaglandin E_2 (PGE_2) is rapidly released through Cx43 hemichannels following fluid flow shear stress and has been shown to increase expression of Cx43 through accumulation of β-catenin and thereby enhance gap junction function and osteocyte communication (28, 36). Cyclooxygenase-2 (COX-2), encoded by the gene *Ptgs2*, is a mechanical load-induced enzyme necessary for the synthesis of prostaglandins (37, 38). Initially, PGE_2 was recognized to induce bone resorption, but it is now known that it also stimulates bone formation (39).

1.2.3.4 Wnt signaling in bone

The canonical Wnt/β-catenin pathway is an important signaling pathway in many tissues, including bone and is activated by secreted Wnt glycoproteins (40). Wnt proteins are known to regulate cellular processes such as differentiation and proliferation of stem cells and progenitors, and cell survival, during both embryonic development and tissue homeostasis (41). Canonical Wnt signaling has an important role in osteoblast differentiation and bone formation, along with BMP signaling and Runx2 (1). The Wnt/β-catenin signaling pathway is also shown to be essential for the skeletal response to mechanical loading. Wnt proteins bind to the transmembrane Frizzled receptor and low-density lipoprotein receptor related protein 5 and 6 (LRP5/6) co-receptor. In the absence of Wnt, the cytoplasmic levels of β-catenin are kept at a low level through proteosomal degradation of β-catenin. The β-catenin destruction complex phosphorylates β-catenin, thus marking it for destruction. The binding of Wnt causes inactivation of the β-catenin destruction complex (40, 42). Following the inactivation of the destruction complex, β-catenin accumulates in the cytoplasm, and is translocated to the nucleus where it acts as a transcriptional co-activator for transcription factor LEF1/TFC, and thus activates the expression of Wnt target genes (40, 41). Various proteins secreted by bone cells can antagonize the canonical Wnt/β-catenin signaling pathway. Sclerostin, a secreted protein encoded by *SOST*, is highly expressed by osteocytes and antagonizes Wnt signaling by binding to LRP5/6 to block Wnt from binding to the co-receptor (43). Sclerostin deficiency causes increased bone mass and bone mineral density (BMD). These findings emphasize the role of sclerostin to inhibit osteoblastic bone formation through decreased Wnt signaling (44). Another protein secreted from osteocytes is Dickkopf1 (Dkk1), also a Wnt signaling antagonist that bind to and block LRP5/6 co-receptor (42, 45).

1.3 Osteocytes as regulators of the bone remodeling process

Osteocytes are long-lived cells, which may live for several decades in bone with low turnover rates. Increased osteocyte apoptosis is associated with withdrawal of estrogen, aging, excess glucocorticoids, increase of pro-inflammatory cytokines, immobilization (unloading), fatigue-loading and radiation (46). Osteocyte cell death increases skeletal fragility and is associated with pathological conditions such as osteoporosis (22). Osteocyte apoptosis can be prevented by mechanical loading, estrogen, intermittent parathyroid hormone (PTH) administration and bisphosphonates (46).

Bone is a dynamic tissue that requires constant renewal and repair throughout life. Bone modeling occur mostly during growth and development, but also in adult life due to adaptations in mechanical load. Unlike bone remodeling, this process is performed by independent actions of osteoblasts and osteoclasts to increase bone mass or reshape bones (47, 48). Bone remodeling occur in response to microdamage that cause osteocyte apoptosis, and results from the sequential actions of osteoclastic bone resorption followed by osteoblastic bone formation, a group of cells that form the basic multicellular unit (BMU) (49). There are three sequential phases of bone remodeling: bone resorption, a transition phase and bone formation (49). The resorption phase begins with migration of pre-osteoclasts to the bone surface where they differentiate and mature. Bone lining cells are retracted from the surface to expose mineralized bone for the osteoclast, which attaches and resorb damaged bone. After this, a transition phase follows where bone resorption is ceased and mononuclear cells prepare the surface for bone formation. In the last phase, osteoblasts secrete osteoid in the resorption cavity, and at last, the surface is covered with bone lining cells to avoid further remodeling (49, 50). Whereas the resorption phase lasts for weeks, the bone formation phase is much slower and takes several months to finish. Mineralization of newly synthesized bone continues long after remodeling is completed (51). There is communication between the bone cells to couple cessation of bone resorption to initiation of bone formation, but the mechanisms of the coupling factors are not fully established.

Osteocytes are considered the orchestrators of bone remodeling. It has been proposed that microdamage in bone impairs the osteocyte cytoplasmic processes and canalicular integrity, an event that induces osteocyte signaling to recruit osteoclasts to initiate local bone resorption and bone remodeling (28). It has been shown that it is the viable osteocytes adjacent to the microcracks that signals osteoclasts, and not the dying osteocytes. The non-apoptotic osteocytes express elevated levels of RANKL, and combined with the low expression of OPG by the

apoptotic osteocytes, an increased RANKL/OPG ratio is observed (52, 53). Osteocytes recruit osteoclasts to the site of remodeling in response to local damage and changes in mechanical load through increased expression of RANKL and release of soluble mediators (23). These mediators include inducers of osteoclastogenesis such as M-CSF, high motility group box protein 1 (HMGB1), vascular endothelial growth factor (VEGF) and pro-osteoclastogenic cytokines (TNF-α, IL-6 and IL-11) (14, 54). MLO-Y4 osteocyte-like cells exposed to pulsatile fluid flow show increased Wnt signaling and inhibition of apoptosis, through opening of cx43 hemichannels and release of PGE_2, insulin-like growth factor 1 (IGF-1) and NO among others. (46, 55). Mechanical load has also shown to reduce expression of the Wnt/β-catenin pathway inhibitor sclerostin significantly, thereby increasing bone formation (56, 57). A simplified figure of bone remodeling regulation by osteocytes is shown in Figure 1.3. In addition to local regulation, bone remodeling processes are regulated by systemic factors, which include PTH, 1,25-dihydroxyvitamin D_3 (calcitriol), glucocorticoids, calcitonin, thyroid hormones and sex steroids (estrogen and androgens) (2).

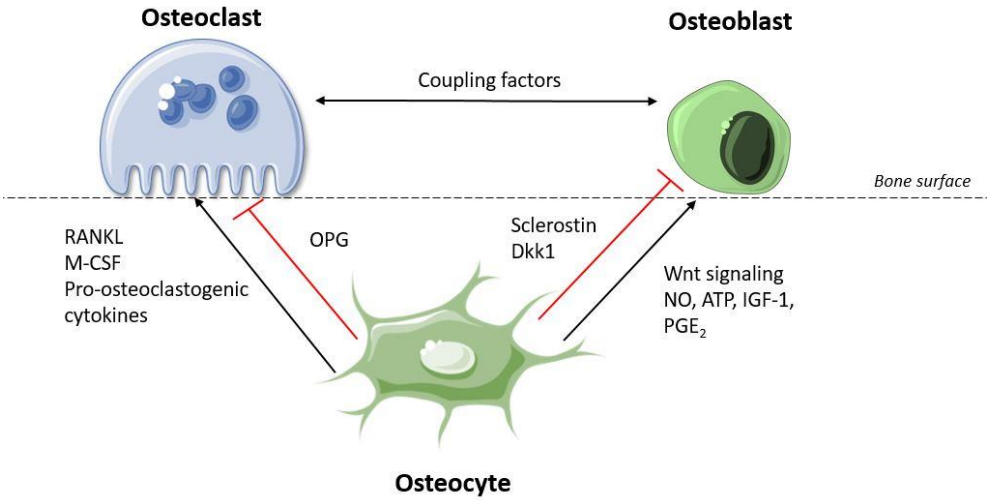

Figure 1.3: Bone remodeling regulation by osteocytes. *Osteocyte expression of RANKL and M-CSF promotes osteoclast activity, whereas OPG inhibits osteoclastogenesis. Osteocyte secretion of PGE_2, NO and ATP promotes osteoblast differentiation and function, whereas secretion of sclerostin and Dkk1 inhibits osteoblasts through blocking Wnt signaling. The figure is created by the author.*

1.4 Osteoporosis

Osteoporosis is a common skeletal disease that increases susceptibility to fractures, characterized by low bone mass, bone fragility and deterioration of bone microarchitecture (58). With an ageing population, osteoporotic fractures constitutes a major public health concern and the incidence of osteoporosis is expected to increase (59). Today, about 40% of white postmenopausal women are estimated to suffer from osteoporosis (60). Scandinavian countries are among the countries with the highest prevalence of hip fractures worldwide. The disease

itself is silent, as it does not cause any symptoms before complications occur. The major complication of osteoporosis is fragility fracture, caused by minor trauma such as falling from standing height or it may happen spontaneously. Osteoporotic fractures are mainly associated with fractures of the hip, spine and wrist, which are bones consisting of higher proportions of cancellous bone. Hip fractures always require hospitalization and are highly associated with increased morbidity and mortality (58).

1.4.1 Risk factors, mechanisms and prevention of osteoporosis

Many local and systemic factors interact to contribute to the increased risk of osteoporotic fractures, but the outcome is the same: bone resorption exceeds bone formation. The most common risk factor is estrogen loss in women at menopause. Estrogen is a key hormone in regulation of bone metabolism, and functions to increase apoptosis in osteoclasts, suppress RANKL and increase OPG. In osteoblasts and osteocytes, estrogen decrease apoptosis, suppress sclerostin and promotes osteoblastogenesis. Decreased levels of estrogen, as seen in postmenopausal osteoporosis, results in an increased rate of bone remodeling, leading to a net bone loss with decreased cancellous bone volume and deterioration of trabecular architecture (61, 62). Although osteoporosis is most common in aging women due to loss of estrogen, it does also occur in aging men (62). Age-related osteoporosis is in contrast to postmenopausal osteoporosis characterized by a decreased rate of bone remodeling (63, 64). Genetic factors, as well as lifestyle are great determinants of bone density. Bone mass peaks in young adults and then gradually declines. Physical activity and particularly weight-bearing exercise is associated with maintenance of peak bone mass and prevention of age-related bone loss, although studies have shown that the effect of high-resistance physical exercise is blunted in postmenopausal women (65-67). Thus, pharmacological treatment should be combined with weight-bearing exercise. In contrast to mechanical load, a sedentary lifestyle and unloading conditions (immobilization or spaceflight) is associated with decreased bone mass (65). Other widely recognized factors that affect bone are medications, including glucocorticoids and diet. Calcium- and vitamin D deficiencies are associated with accelerated bone loss, and an adequate daily dietary intake of calcium and vitamin D prevents bone loss (62, 68).

1.4.2 Radiation therapy-induced osteoporosis

Osteoporosis is a frequent complication of radiation therapy (RT) in cancer patients. RT-induced osteoporosis is often observed in patients treated for pelvic cancers, including cervical, rectal and anal cancers. It is demonstrated that these patients have reduced BMD and a substantially increased risk of hip fracture (69, 70). Although ionizing radiation mainly targets

fast-dividing cancer cells, healthy cells are also affected, including bone cells. The effect of radiation in bone is not completely understood, but appear to be due to an acute period of osteocyte apoptosis and bone resorption, followed by a long-term suppression of osteoblasts that prevent recovery of bone mass (71). The damage appear to be greater in cancellous than cortical bone, and cancellous bone loss is identified 3 days after γ-radiation in doses down to 2 Gy (72, 73). The SI unit Gray (Gy = joule/kg) is a measure of absorbed dose of radiation (74). Recent studies show that RT stimulates osteoclastogenesis and osteoclast function through increased expression of RANKL and pro-osteoclastogenic cytokines, and decreased OPG expression in irradiated MLO-Y4 osteocytes. The MLO-Y4 cells displayed reduced viability 3 days following a radiation dose of 4 Gy, indicating that radiation induces osteocyte apoptosis (75). Radiation appears to increase sclerostin secretion by osteocytes, which exerts an inhibitory effect on osteoblastic bone formation (76). Following radiation, it has been shown that the potential of osteogenic potential of MSC is severely damaged, leading to a decrease in the number and activity of osteoblasts (77). As of today, the current treatment is conventional antiresorptive drugs in addition to physical activity and sufficient intake of calcium and vitamin D (78).

1.4.3 Pharmacological treatment of osteoporosis

The most common treatment of osteoporosis is the use of antiresorptive agents. These include bisphosphonates, RANKL-antibodies, estrogen replacement, selective estrogen receptor modulators, with bisphosphates normally being first line therapy. Bisphosphonates acts by binding to hydroxyapatite on bone surfaces, and is released upon bone resorption where it inhibits osteoclast function. Thus, bone resorption is inhibited and the bone turnover rate is reduced (79). Denosumab is a monoclonal antibody that binds to RANKL, similar to OPG. Considering RANKL is a master regulator of osteoclast formation and function, antibodies towards RANKL disrupt osteoclastogenesis and limit bone resorption, resulting in increased bone density (62). The recombinant human PTH analog teriparatide is one of the only approved bone anabolic agents in use, and acts by increasing bone formation and BMD if administered intermittently (58, 80). The abovementioned treatments have to be discontinued after few years and some have possible serious side effects. Potential new treatments for osteoporosis include sclerostin inhibitors (bone anabolic agent) and cathepsin K inhibitors (antiresorptive agent) (58, 62). The antihyperglycemic AMPK-activating agent metformin has also been proposed to have beneficial effects in bone.

1.5 AMP activated protein kinase (AMPK)

AMPK is an intracellular energy sensor important for maintenance of cellular energy homeostasis (81). Recently, it has been suggested to play a role in bone physiology and especially the AMPK activator metformin has gained a lot of attention.

1.5.1 Structure, activation and regulation

AMPK is a heterotrimeric enzyme complex, consisting of α, β and γ subunits. The α-subunit has an important catalytic domain with ser/thr kinase activity, necessary for activation of the complex. (82). The regulatory β-subunit has a carbohydrate-binding molecule, and functions as a scaffold for α and γ subunits, in addition to defining the substrate specificity and defining the subcellular localization of AMPK. The γ-subunit is also regulatory and has a nucleotide-binding site to allow competitive AMP- and ATP binding (82-84). Mammalian AMPK subunits are encoded by seven distinct genes, encoding two α-subunits, two β-subunits and three γ-subunits(84), yielding a total of 12 different combinations. A distinct heterotrimer in a specific tissue can determine the effects of drugs in the tissue in question (85).

There are several factors leading to the activation of AMPK, such as environmental or nutritional stress, that results in depletion of intracellular ATP. Examples are exercise, starvation, hypoxia, inhibition of mitochondrial respiration by metabolic poison and through mechanisms of drugs such as metformin, thiazolidinediones (TZDs) and 5-Aminoimidazole-4-carboxamide ribonucleotide (AICAR) (82, 86). The result of the increased cellular energy demand is an increased AMP/ATP and ADP/ATP ratio, which activates AMPK. This switches on energy-generating (catabolic) pathways and switches off energy-consuming (anabolic) pathways (Figure 1.4) (86). If anabolic pathways are required, AMPK is kept at a low level of activation (82). Upon the increased AMP/ATP ratio, AMP or ADP binds to the γ-subunit of the AMPK complex and thereby promotes phosphorylation of Thr172 by the major upstream kinase LKB1 (82). The binding of AMP inhibits dephosphorylation of Thr172 through a conformational change of AMPK (87, 88). In addition, binding of AMP results in allosteric activation of AMPK (82). ATP inhibits all the three activation mechanisms, and explains why AMPK acts as a sensor of energy homeostasis. Although it is not the major pathway of activation, AMPK can also be activated by nucleotide-independent mechanisms. Metabolically relevant hormones, such as ghrelin and adiponectin, increase the concentration of intracellular $Ca^{2+,}$ which results in Thr172 phosphorylation of α-subunit by upstream kinase CAMKK2 (82, 89). A non-canonical pathway of activation does also exist, and includes activation triggered

by reactive oxygen species (ROS) and genotoxic treatments such as ionizing radiation and DNA-damaging drugs (90).

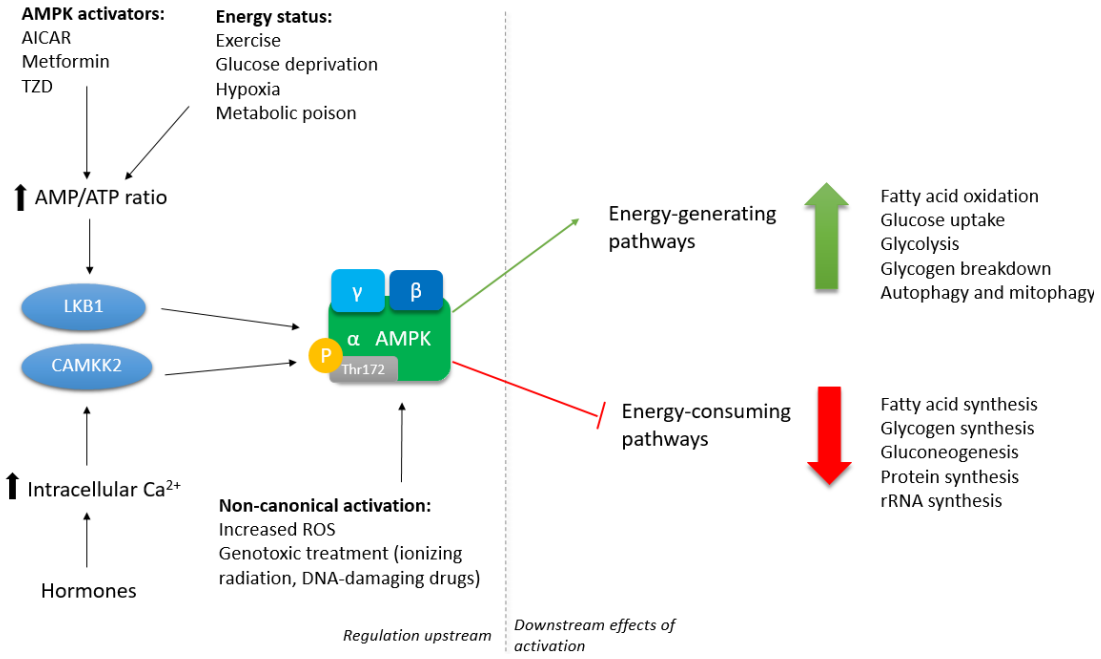

Figure 1.4: Activation of AMPK and downstream metabolic effects. *AMPK is activated by increased AMP/ATP ratio and increased intracellular Ca^{2+} during cellular energy stress, which switches on energy-generating pathways and switches off energy-consuming pathways. The figure is created by the author.*

1.5.2 Effects of AMPK activation

The main sources of energy supply and storage in cells are glucose and lipids. ATP is generated through activation of AMPK by inducing breakdown and inhibition of synthesis and storage of these macromolecules (82). The catabolic pathways stimulated by AMPK activation include promotion of glucose uptake with subsequent generation of ATP through glycolysis (90). Furthermore, AMPK inhibits glycogen synthesis and activates glycogen breakdown (91). The hepatic gluconeogenesis, important for maintenance of blood glucose levels through glucose synthesis is reduced, and insulin sensitivity is improved (82, 84, 91). Regarding lipid metabolism, AMPK promotes fatty acid uptake and subsequent breakdown through fatty acid oxidation in the mitochondria, as well as suppression of de novo fatty acid synthesis and cholesterol synthesis (82, 91). Protein synthesis is highly energy demanding, and is inhibited by AMPK to conserve cellular ATP through inhibition of the mTOR complex, proteins involved in protein translation and synthesis of rRNA (82, 91). AMPK promotes autophagy in response to states of low cellular energy and likewise, AMPK is shown to induce degradation of defective mitochondrial components (mitophagy) upon sustained energy stress and mitochondrial damage (82). AMPK is a regulator of appetite, and contributes in the control of whole-body energy homeostasis through hypothalamic actions by hormones such as ghrelin, adiponectin

and leptin (90, 92). AMPK is a mediator in non-metabolic pathways, which includes inhibition of cell growth, proliferation and oxidative stress response, in addition to anti-cancer and anti-inflammatory properties (82, 90). Recently, AMPK signaling has been shown to play a role in bone physiology.

1.6 AMPK in bone physiology

In bone, α_1 is the predominant α-subunit and is highly expressed in both osteoblasts, osteoclasts, and in cell lines of the osteoblastic lineage, which implies that it has a considerable function in bone. The expression of α_2-subunit in bone is low. Both β-subunits are expressed in bone, whereas γ_1-subunit is the major γ-subunit in bone cells (81, 93). AMPKα_1 knock out mice display decreased bone mass compared to the wild-type, both in trabecular and cortical bone, whereas mice with AMPKα_2 knock out show no significant change in bone parameters and do not seem to be critical for bone metabolism (93). In agreement with this, mice with AMPKα_1 deletions showed increased rates of bone remodeling, which favors bone resorption (94). Mice with germline deletions of AMPKβ_1 and β_2 has been shown to exhibit a low bone mass phenotype compared to the wildtype (95). Several in vitro studies have shown that the AMP mimetic AICAR activates AMPK in both osteoblasts and osteoclasts, supporting a role of AMPK in bone metabolism.

1.7 Metformin – an AMPK activating agent

Besides AMPK activators such as exercise and glucose deprivation, drugs including AICAR and metformin activate AMPK. Whereas AICAR act as an AMP mimetic to activate AMPK, metformin act primarily by increasing the AMP/ATP ratio (82). Metformin is an oral antidiabetic drug in the class of biguanides, and is widely used in the treatment of type 2 diabetes. The main anti-hyperglycemic effects of metformin include decreased hepatic glucose production and increased insulin sensitivity in several tissues, which improves glucose uptake into cells and consequently lowers blood glucose levels (96). Although it has been in use for several decades, the mechanisms are not completely understood. Metformin is thought to activate AMPK through inhibition of complex 1 in the mitochondrial respiratory chain, which inhibits ATP production, thus resulting in an increased AMP/ATP ratio (97). AMPK activation might not explain all therapeutic effects of metformin, and several AMPK-independent mechanisms are proposed (90). It is demonstrated that one AMPK-independent mechanism is the inhibition of fructose-1,6-bisphosphatase by the increased AMP levels, which directly limits gluconeogenesis in the liver (98). Compared to other antidiabetic drugs that may play roles in bone physiology, metformin is reported to not have any effects on the glucose levels in non-

diabetic individuals. In addition, metformin is considered safe because it does not have any major side effects aside from gastrointestinal irritation and rarely lactic acidosis may occur. Therefore it is suggested that metformin can be used as an adjuvant osteoporosis therapy (97).

1.8 Effects of metformin and AMPK activation on bone

Few clinical studies reporting skeletal effects of metformin are published, but several epidemiological studies are available, reporting effects of diabetes and metformin treatment on the risk of bone fracture. Diabetes mellitus is reported to be associated with an increased fracture risk. A case-control study on diabetic patients in Denmark reported that the use of metformin significantly decreased fracture risk compared to other antidiabetic medications at any site, and this is later confirmed by several other population-based studies (99-101). However, other studies have not found any association between metformin and fracture risk (102).

Several studies implies that activation of AMPK stimulate bone formation. In 2006, the first study to investigate bone cell actions of metformin demonstrated osteogenic effects on osteoblasts in vitro (103). Later, Shah et al. demonstrated that AMPK activation by metformin leads to bone nodule formation, but when treated with the AMPK inhibitor compound C, bone formation was reduced (93). Moreover, it is reported by Kanazawa et al. that differentiation and mineralization of MC3T3-E1 osteoblasts is stimulated by metformin through inhibition of the mevalonate pathway, which is a known effect of AMPK activation. The cells showed increased expression of osteoblast markers, including type 1 collagen, osteocalcin and ALP activity, and these results were later confirmed by several studies (104, 105). Additionally, Zhen et al. reported decreased ROS, osteoblast apoptosis and increased osteoblast markers following hyperglycemia when cultured primary osteoblasts were stimulated with metformin, reversing the destructive effects of high glucose levels (106).

More recent, overexpression of AMPK was reported to stimulate osteogenesis in MC3T3-E1 osteoblastic cells and to inhibit adipogenesis in 3T3-L1 adipocytes (107). AMPK activation by AICAR and metformin is reported to stabilize Runx2, and regulate Wnt/β-catenin signaling through stabilization of β-catenin, thus promote differentiation of MSCs into the osteoblastic lineage (108, 109). Molinuevo et al. studied the effects of metformin treatment in bone marrow progenitor cells (BMPC). They demonstrated that metformin phosphorylate AMPK in undifferentiated BMPCs, and had an osteogenic effect both in vitro an in vivo, conceivably through Runx2-mediated actions (110). Wnt signaling suppress peroxisome proliferator-activated receptor gamma (PPARγ), which is a critical factor for adipocyte commitment and

differentiation. Consequently, AMPK activity decrease adipogenesis. Conversely, PPARγ suppress osteoblastogenesis, partly demonstrated by the detrimental effects PPARγ agonist TZD has on bone mass (96, 111, 112). In contrast to studies that has reported osteogenic effects of metformin, Kasai et al. demonstrated that differentiation of osteoblasts is associated with decreased phosphorylation of AMPKα and that metformin inhibits osteoblast differentiation and significantly downregulate Runx2 and osteoblast differentiation markers (113). Overall, studies indicate that metformin is able to activate AMPK in osteoblasts and have beneficial effects on osteoblastic bone formation.

Although most studies on metformin and bone are performed on osteoblasts, several lines of evidence supports a role for AMPK in osteoclastogenesis. Lee et al. demonstrated that metformin activation of AMPK suppresses osteoclastogenesis induced by RANKL, and that pharmacological inhibition of AMPK enhances osteoclastogenesis and bone resorption (114). A study performed on ovariectomized rats, associated by increased bone loss due to estrogen withdrawal, demonstrated decreased bone loss when treated with metformin (115). Another study showed reduced expression of RANKL and increased OPG expression by osteoblasts in response to AMPK activation by metformin, both in ovariectomized rats and in cultured cells (116).

Recently, Stunes et al. investigated the effect of metformin and exercise in ovariectomized rats. Their results indicate that both metformin and exercise both reduces bone resorption in rats, but do not show an additive effect when combined, although they appear to improve trabecular microarchitecture compared to the ovariectomized control (117). In contrast to previous studies, Jeyabalan et al. reported that ovariectomized mice treated with metformin showed no effect on bone resorption, but instead a decreased rate of bone formation in cancellous bone. Additionally, they demonstrated that metformin did not affect bone fracture healing in mice (118). Overall, results indicate that metformin suppress osteoclastogenesis, bone resorption and bone loss.

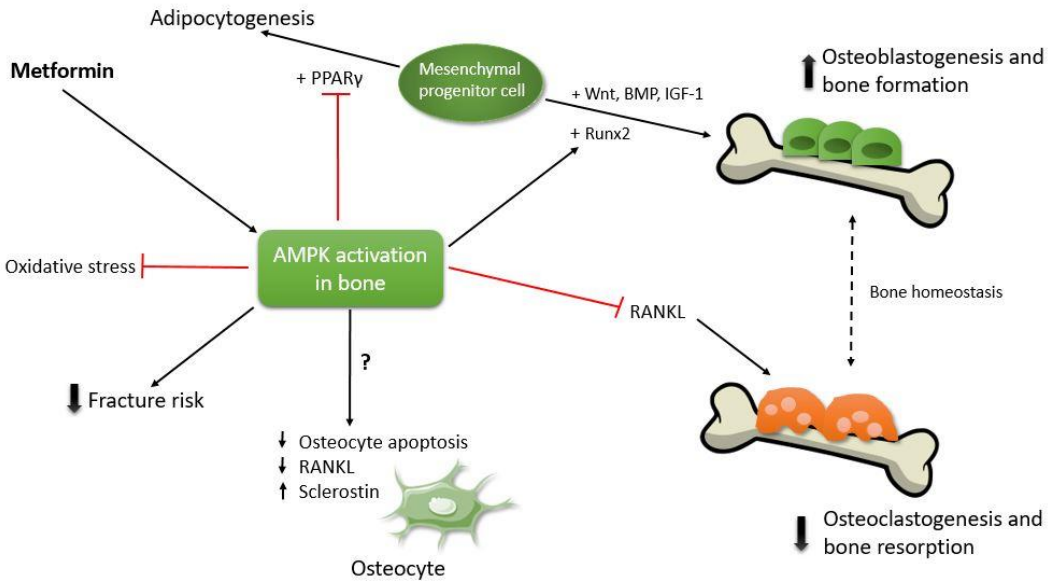

***Figure 1.5: AMPK and bone metabolism**. Metformin activates AMPK in bone, resulting in decreased bone resorption by osteoclasts and increased bone formation by osteoblasts, which decreases osteoporotic fractures. Metformin is also thought to have effects in osteocytes, but more studies are needed to reveal the mechanisms. The figure is made by the author.*

Even though the majority of studies focus on other bone cells, it is thought that AMPK can be activated in osteocytes (Figure 1.5). Takeno et al. recently demonstrated MLO-Y4 express all seven AMPK subunits (119). They did also report that metformin has anti-apoptotic effects against homocysteine-induced apoptosis in MLO-Y4 osteocytes through AMPK-dependent mechanisms against oxidative stress (119). Next, the same research group investigated the effects on RANKL and sclerostin expression in MLO-Y4 by the AMPK activator AICAR. They found that AMPK activation resulted in an increased mRNA and protein expression of sclerostin, whereas RANKL expression was reduced, through inhibition of the mevalonate pathway.

2. Aim of study

There is a need for further studies to investigate the role of AMPK activation in osteocytes, to provide new insights on the effects on bone metabolism, and whether metformin could be a potential adjuvant therapy for osteoporotic bone disorders, similar to exercise. Therefore, the main aim of the study was to investigate the effects of the AMPK-activating compound metformin on osteocyte survival, in addition to studying gene and protein expressions of markers associated with mechanical load response in osteocytes in vitro. Considering both exercise and metformin are AMPK-activators, it was of interest to investigate whether metformin mimics the effect of mechanical load in osteocytes. The murine osteocyte-like cell line MLO-Y4 was chosen as a model system for this study.

The second aim of the study was to investigate the effect of metformin on apoptosis in MLO-Y4 osteocytes exposed to ionizing radiation, considering that patients undergoing radiation therapy are at risk of developing RT-induced osteoporosis, and new adjuvant therapies are needed.

3. Materials and methods

3.1 Cell culture

Murine long bone osteocyte Y4 cells (MLO-Y4) was the cell line used in this study and was provided by Lynda F. Bonewald, University of Missouri, USA. The cell line is obtained from isolated osteocytes from the femur and tibia of 14-day-old transgenic mice immortalized by the use of the osteocalcin promoter that drives the large T antigen (120, 121). The MLO-Y4 osteocytes were maintained in minimum essential medium alpha (MEM-α) (Gibco), supplemented with 5% calf serum (CS) (Sigma-Aldrich), 5% fetal calf serum (FCS) (Gibco), 4 mM L-glutamine (Gibco), 10 U/mL Penicillin/Streptomycin (Gibco), 0.1 mg/mL fungizone (Gibco) and 1.5 g/L Na-pyruvate (Gibco). This will be further referred to as normal growth medium.

For the cells to attach properly, they were maintained in collagen coated flasks (0.15 mg/mL, Discovery Labware Inc) and grown until ~70 % confluency before they were split 1:3-1:5 (every 3-4 days). The cells were incubated at 5 % CO_2 and 37 °C.

3.1.1 Subculturing of MLO-Y4 cells

To split the cells, growth medium was removed from the cells and they were washed once with 3 mL trypsin (0.05% trypsin/0.5 mM EDTA solution) (Lonza). Thereafter, 3 mL trypsin was added to detach the cells for approximately 3 minutes at 37 °C. Normal growth medium was added to the cells up to a total volume of 10 mL to stop the trypsin reaction and the cells were centrifuged for 5 minutes at 800 rpm. The medium was removed, and the cells were resuspended in growth medium. Considering the cells prefer their own conditioned medium, centrifuged conditioned were added to the growth medium when seeding new flasks.

3.1.2 Collagen coating

The collagen solution was prepared by diluting sterile type 1 rat tail collagen (Discovery Labware Inc) in 0.02 M acetic acid to a concentration of 0.15 mg/mL. A chilled pipet was used for the coating to avoid collagen adhering to the pipet walls. After addition of collagen, a one-hour incubation in room temperature was necessary for the collagen to adhere to the surface. Excess collagen was removed and the plates were left in the incubator overnight to dry before storage at 4 °C.

3.1.3 Thawing of cells

Frozen cells were stored in 90 % FCS and 10 % DMSO in liquid nitrogen. Upon thawing, high serum growth media (10% FCS and 10% CS) was added to the cells immediately after they

were thawed in a water bath, and the cells were centrifuged for 5 minutes at 800 RPM. The cells were resuspended in high serum growth media and seeded in T75 flasks.

3.1.4 Preparation of metformin dilutions

The anti-diabetic drug metformin used in all experiment was purchased from Chiron Norway. For all experiments, the metformin dilutions used were 0 µM (control with no metformin), 100 µM, 500 µM and 2000 µM. Metformin was diluted in low serum media (MEM-α supplemented with 1 % FCS) from a stock solution of 100 mM.

3.2 Lactate dehydrogenase (LDH) activity assay

A LDH activity assay was performed to study the cytotoxicity of metformin in MLO-Y4 osteocytes. Following damage to the plasma membrane of cells, the cytoplasmic enzyme LDH, is released into the extracellular space. In the first step of the reaction, NAD^+ is reduced to $NADPH/H^+$ by LDH and lactate is converted to pyruvate, as illustrated in Figure 3.1. In the next step, the H/H^+ is transferred to the tetrazolium salt INT, which then is reduced to formazan. The increase of extracellular LDH is proportional to the amount of formazan formed in the reaction, and thereby the optical density is proportional to the number of lysed cells in the sample (122, 123).

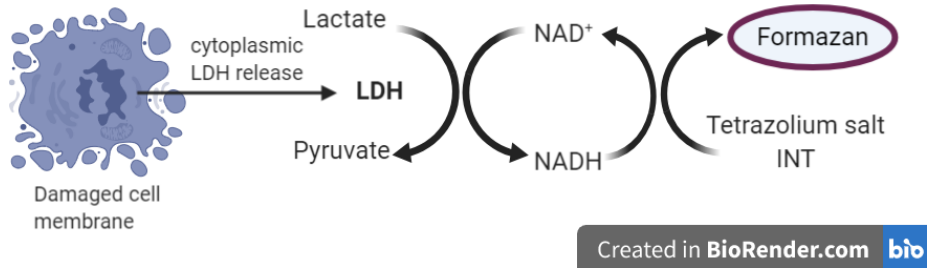

Figure 3.1: Principle of LDH activity assay. *Upon cytotoxic damage, LDH is released from the cytoplasm, which leads to reduction of NAD^+, converting lactate to pyruvate. The reduction of NAD^+ leads to transfer of H/H^+ to formazan, which is measured by its optical density. The optical density of the end-product reflects the amount of damaged/dead cells in the samples. The figure is created by the author at biorender.com*

The cells were seeded at a density of 2500 cells/well in 100 µL normal growth medium in 96-well plates. After 24 hours, the normal growth medium was changed to low serum media with or without metformin (100µM, 500 µM and 2000 µM) in four replicates. The medium was collected after 24- and 48-hour exposure to metformin and was centrifuged to remove cell debris before 50 µL was transferred to new plates. RIPA lysis buffer (10 µL) was used as a high control to reach maximum LDH release and was added 15 minutes before the medium was collected after 48 hours. To examine the LDH release, a LDH cytotoxicity kit (Roche) was utilized, following the manufactures protocol (Appendix 1). Instead of using 100 µL of medium

sample, 50 µL was used and therefore the reagent mix volume was reduced to 50 µL. The samples were incubated for 15 minutes in the dark before 50 µL 1M acetic acid was used to stop the colorimetric reaction. The absorbance was measured at 490 nm using a BioRad microplate reader.

3.3 Harvesting and RNA isolation of metformin stimulated cells

MLO-Y4 cells were seeded in 6-well plates at a density of 150 000 cells/well in 2 mL normal growth media. After 48 hours, media was changed to low serum media and metformin (0 µM, 100 µM, 500 µM and 2000 µM) in triplicates for each time point. The cells were harvested after 24, 48 and 72 hours. Medium was saved for protein experiments. After 48 hours, the medium and conditions were changed for the remaining cells.

To harvest the cells, medium was removed, and the cells were washed twice with cold phosphate-buffered saline (PBS). The cells were then disrupted by adding 350 µL/well of RLT lysis buffer (Qiagen), containing β-mercaptoethanol to denature RNases. Cells were lysed using a 20G needle and syringe before storage at -80 °C. Total RNA was isolated using the QIAGEN RNeasy Mini Kit according to the protocol from the manufacturer (Qiagen) (Appendix 2). For elution, a volume of 20 µL RNase free water was used. As the expected RNA yield was under 30 µg, the last step of the protocol was not performed. To avoid degradation of RNA by RNases, the protocol was performed under RNase-free conditions. RNA concentration and quality were measured on the DeNovix Spectrophotometer DS 11 before RNA was stored at -80 °C.

3.4 cDNA synthesis

Isolated total RNA from metformin-stimulated MLO-Y4 osteocytes was converted to more stable complementary DNA (cDNA) for further use. The reaction follows the principle of reverse transcription, where single stranded RNA is transformed to double stranded DNA using the enzyme reverse transcriptase (RT) and either a primer complementary to the 3' end of the RNA or random hexamer primers that bind to random complementary sites at target RNA (124).

Thermo Scientific Maxima First Strand cDNA synthesis kit for RT-qPCR (Thermo Scientific) was used for the cDNA synthesis. Each reaction was prepared as described in Table 3.1. The total reaction volume was 20 µL per RNA sample. RNA samples and the enzyme mix were kept on ice during the reaction preparation. Samples were then mixed gently and incubated for 10 minutes at room temperature, 15 minutes at 50 °C and finally 5 minutes at 85 °C to stop the reaction. cDNA from three technical replicates of each condition and time point were pooled and diluted 1:3 in nuclease-free water. cDNA was stored at -20 °C.

Table 3.1: cDNA synthesis reaction setup.

Component	Volume/amount per reaction
5x reaction mix	4 µL
Maxima enzyme mix	2 µL
RNA sample	100 ng
Nuclease free water	Up to a total of 20 µL

3.5 Quantitative polymerase chain reaction (qPCR)

qPCR was performed to assess the relative mRNA expression of *Piezo1*, *Sost*, *Ptgs2*, *RANKL*, *OPG*, *Wnt3a and Wnt1* after metformin stimulation of MLO-Y4 cells. The primers were purchased from BioRad and are shown in Table 3.2. qPCR allows analysis of gene-specific mRNA expression, and the method used to detect amplicons in this experiment was fluorescent SYBR green. This molecule binds non-specifically within double stranded DNA exclusively, which allows simultaneous amplification and quantification (125).

Table 3.2: Primer information for genes used in qPCR reaction*. For commercial primers where the sequence is not available, the assay ID from the manufacturer (Bio-Rad) is shown.*

Target genes	Forward sequence (5' to 3')	Reverse sequence (3' to 5')	Amplicon size	Sequence ID	Assay ID
GAPDH	AATGGGGTGA GGCCGGTGCT	CACCCTTCAA GTGGGCCCCG	87 bp	NM_009094.2	
Sost			62 bp	NM_024449.6	qMmuCED0045167
Ptgs2			107 bp	NM_011198.4	qMmuCED0047314
Piezo1	GCGGCGCTAT GAGAACAAG	CTGCGAGCGG TGGAAGA	118 bp	NM_001357349.1	
Wnt1			100 bp	NM_021279.4	qMmuCED0046180
Wnt3a	TAGATGGGTG CGACCTGTTG	GAACCCTGCT CCCGTGTTAG	177 bp	NM_009522.2	
OPG			156 bp	NM_008764.3	qMmuCID0027158
RANKL			194 bp	NM_011613.3	qMmuCID0026078

The qPCR reaction mix was made as described in Table 3.3 and added to 96-well qPCR plates. PerfeCTa SYBR Green FastMix (2x) was purchased from Quantabio. Standards were run in triplicates and samples were run in duplicates. The plate was covered in qPCR compatible adhesive film and centrifuged for 30 s for removal of air bubbles. Standard curves were prepared for each gene by using serial dilution from a pool of cDNA samples in relative concentrations (1, 0.5, 0.2, 0.1, 0.05, 0.02, 0.01 and 0.005). The use of standard curves enable relative quantification of sample cDNA input (126). Glyceraldehyde 3-phosphate dehydrogenase (*GAPDH*) was used as a reference gene, and all genes were normalized to *GAPDH* for correction of variations in amount of RNA in the samples.

Table 3.3: qPCR reaction mix setup.

Component	***Volume***	***Volume (GAPDH)***
Primer (0.2 µM final concentration)	1 µL	1 µL forward primer 1 µL reverse primer
PerfeCTa SYBR Green FastMix (2x)	10 µL	10 µL
Nuclease-free water	7 µL	6 µL
Standard or sample	2 µL	2 µL
Total volume of qPCR reaction mix	20 µL	20 µL

The instrument StepOnePlus™ Real-time PCR (Applied Biosystems) was used for amplification and quantification. The cycling parameters were set to 95°C (10 minutes) at the holding stage, and in the cycling stage the parameters were set to 95 °C (15 seconds) to denature dsDNA and then lowered to 60 °C (60 seconds) for annealing and elongation of DNA. These two steps were repeated for a total of 40 cycles. In the melt curve stage, the temperature was gradually increased +0.3 °C up to 95 °C and fluorescence was measured at each increase in temperature. The melting curve was included to ensure no amplification of non-specific PCR products.

3.6 Prostaglandin E_2 (PGE_2) ELISA

To assess the secretion of PGE_2 from metformin-stimulated MLO-Y4 cells, the prostaglandin E_2 enzyme-linked immunosorbent assay (ELISA) monoclonal kit (Item No. 514010) from Cayman chemicals was used. The kit is a monoclonal competitive ELISA assay, based on the competition of PGE_2 in the sample and a PGE_2-acetylcholineesterase (PGE_2-AChE) conjugate tracer for a small amount of PGE_2 antibody. The plate is coated with goat-anti mouse IgG in which PGE_2-antibody complexes bind. To remove unbound components, the plate is washed before development with Ellman's reagent, the substrate for the AChE tracer. This yields a yellow color that can be measured photometrically, and the color intensity is inversely proportional to the amount of PGE_2 in the sample. The reaction principle is illustrated in Figure 3.2.

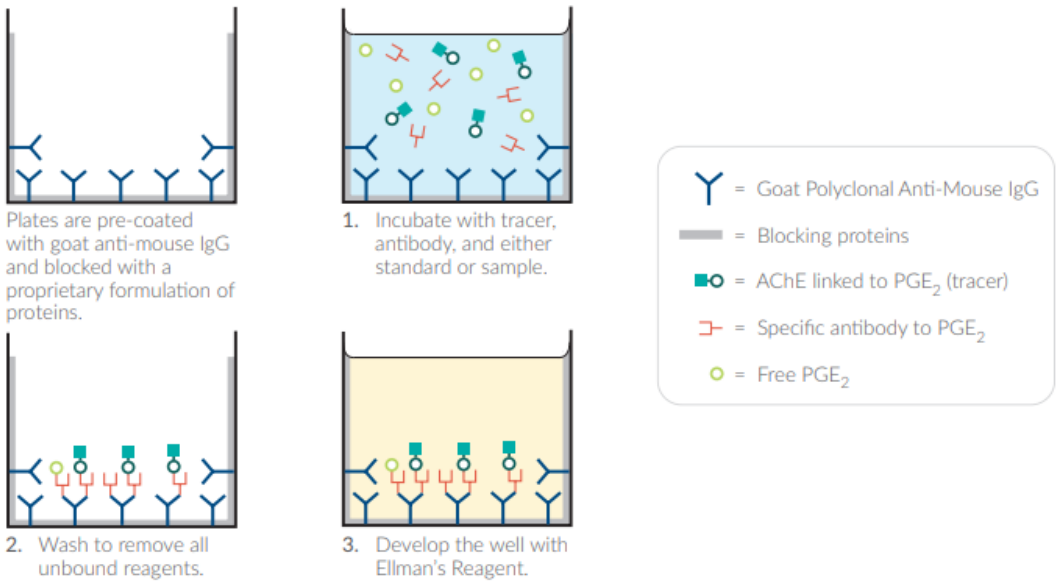

***Figure 3.2: Principle of competitive ELISA**. PGE2-AChE tracer, antibodies towards PGE2 and sample is added to the anti-mouse IgG antibody coated plate. PGE2-AChE tracer and PGE2 in the sample competes for PGE2 antibodies. PGE2-antibody complexes bind to antibodies in the plate, and unbound reagents are washed away. Ellman's reagent act as a substrate and gives a yellow color that can be measured. The figure is from the manufacturers protocol (127).*

Medium was collected from the MLO-Y4 cell experiments in 6-well plates treated with metformin, previously described in 3.3. The medium was centrifuged to remove cell debris, and supernatants from three technical replicates were pooled. The medium samples were diluted 1:10 in ELISA buffer. A standard curve was prepared in ELISA buffer according to the manufacturer's protocol. Both standards and samples were run in duplicates. Samples, standards, tracer and antibodies were added to the plate following the manufacturer's protocol (Appendix 3). The TA (total activity) wells were left out in this experiment. The plate was incubated overnight at 4 °C and washed 5x with wash buffer, before development with 200µL

Ellman's reagent in each well. Before absorbance readings, the plate was incubated in the dark for 60 minutes on an orbital shaker. The plates were read at 415 nm on a BioRad microplate reader. PGE_2 concentrations were calculated using a four-parameter fit standard curve.

3.7 MTT proliferation assay

A 3-(4,5-dimethylthiazol-2-yl)-2,5-diphenyl tetrazolium bromide (MTT) proliferation assay was performed to assess whether metformin stimulates cell proliferation. The kit CellTiter 96 Non-radioactive proliferation assay (Promega) was used for this purpose. MTT is a tetrazolium salt that is cleaved into insoluble formazan crystals in metabolically active mitochondria and makes the assay suitable for measurement of the number of living cells (Figure 3.3) (128). After a solubilization step, the formed formazan product can be measured based on its optical density, and the absorbance is directly proportional to the number of living cells.

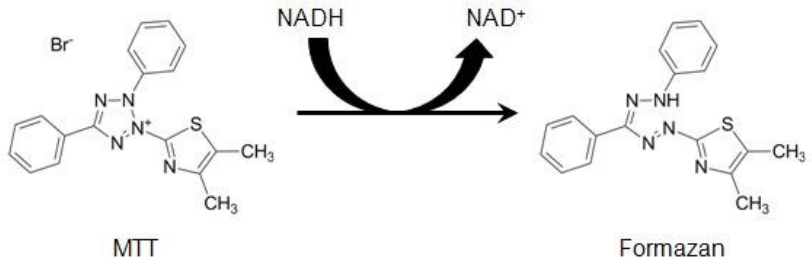

Figure 3.3: Principle of MTT assay. *The tetrazolium salt MTT (3-(4,5-dimethylthiazol-2-yl)-2,5-diphenyl tetrazolium bromide) is converted to purple formazan crystals, which is proportional to the number of metabolically active cells. The figure is from Riss et al. (129).*

MLO-Y4 cells were seeded 1000 cells/well in 96-well plates in 200 µL normal growth medium. After 24 hours, the medium was changed to 100 µL low serum medium with or without metformin (100µM, 500µM and 2000µM). Then, after 24-, 48-, and 72 hours, 15 µL of the dye solution (MTT) was added to the wells. The cells were then incubated for three hours at 37 °C 5% CO_2 before 100 µL solubilization solution (10 % SDS, 0.001 N HCl) was added to the wells to form soluble formazan. The plates were then incubated for 24 additional hours at 37 °C before the content of the wells were transferred to a new plate and stored at 4 °C until all plates were ready. Absorbance was read at 570 nm with a reference wavelength of 655 nm.

3.8 Radiation of metformin-stimulated cells

To investigate whether metformin could prevent radiation-induced apoptosis, MLO-Y4 cells were seeded in two 96-well plates in a density of 5000 cells/well in 100 µL normal growth Metformin was added in doses of 0 µM, 100 µM, 500 µM and 2000 µM in 100 µL low serum

media after 24 hours, immediately before radiation. A linear accelerator was used to irradiate the cells in an absorbed dose of 5 Gray (Gy), by acceleration of particles, which creates high energy photon radiation (high energy x-rays) (130). Non-irradiated cells (0 Gy) with or without metformin was used as the control group.

3.9 Cell death detection ELISA assay

To examine the extent of apoptosis of metformin-stimulated irradiated MLO-Y4 osteocytes, the cell death detection ELISA^{PLUS} kit (Cat. No 11774425001; Roche), based on a quantitative sandwich ELISA principle was used. The method allows specific determination of mono- and oligonucleosomes in cell lysates, which is an indicator of apoptosis initiation.

When a sample is added to the streptavidin-coated microplate and monoclonal anti-histone (biotin conjugated) and anti-DNA (Horse radish peroxidase (HRP) conjugated) antibodies are added, the specific antibodies bind to nucleosome-associated histones and DNA in the sample, respectively. The newly formed immunocomplex binds to the streptavidin-coated microplate, and unbound components are washed away. HRP retained in the immunocomplex allows quantification of nucleosomes in the sample through addition of ABTS substrate, which binds to HRP and yields a green end-product that can be measured photometrically (Figure 3.4) (131).

The irradiated cells were analyzed following the manufactures protocol (See Appendix 4) with five replicates for each condition. A positive control was included. The samples were incubated for 15 minutes after addition of the ABTS substrate and were measured at 405 nm with a reference wavelength of 490 nm.

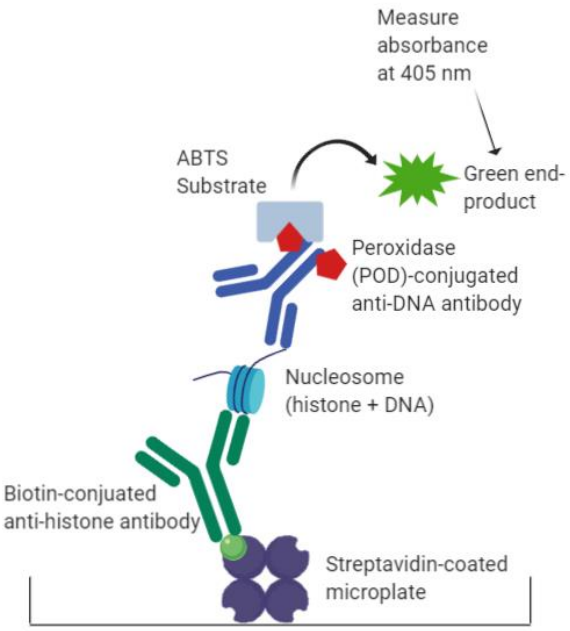

Figure 3.4: Principle of ELISA cell death detection assay. *Anti-histone-biotin and anti-DNA-POD binds to the histone and DNA fragments on the nucleosome, respectively, and form an immunocomplex. The biotin-conjugated anti-histone antibody binds to the microplate through streptavidin, and the ABTS substrate binds to the peroxidase-conjugated anti-DNA antibody and generates a green end-product which can be measured optically. The figure is created by the author on biorender.com*

3.10 Statistical analysis

Unpaired two-tailed student T-tests were used for statistical purposes and metformin-treated cells were compared to non-treated controls. Error bars represent standard error of the mean (SEM) or standard deviation (SD) and graphs were made in GraphPad Prism 8. Results were considered statistically significant if P-values <0.05 (*).

4. Results

4.1 Metformin does not increase LDH release in MLO-Y4 cells

First, it was of interest to establish that metformin is not toxic to the MLO-Y4 in the concentrations that were chosen for the further experiments. For this, an LDH activity assay was performed, which measures membrane damage and necrotic cell death through release and activity of cytoplasmic LDH. MLO-Y4 osteocytes were cultured as described above, +/- metformin (100, 500 and 2000 µM for 24 and 48 hours). RIPA lysis buffer was added to control cells for lysis of the cells and subsequent LDH release, to verify that the assay was working properly. The results of the LDH activity assay show that metformin did not cause a higher release of LDH in none of the concentrations at the time points that were used. In contrast, metformin significantly ($p<0.01$) decreased LDH activity in the cells treated with 100 µM metformin after both 24 and 48 hours, compared to the untreated control (Figure 4.1). The positive control (RIPA lysis buffer) displayed a 2-4-fold increase in LDH activity compared to control (not shown).

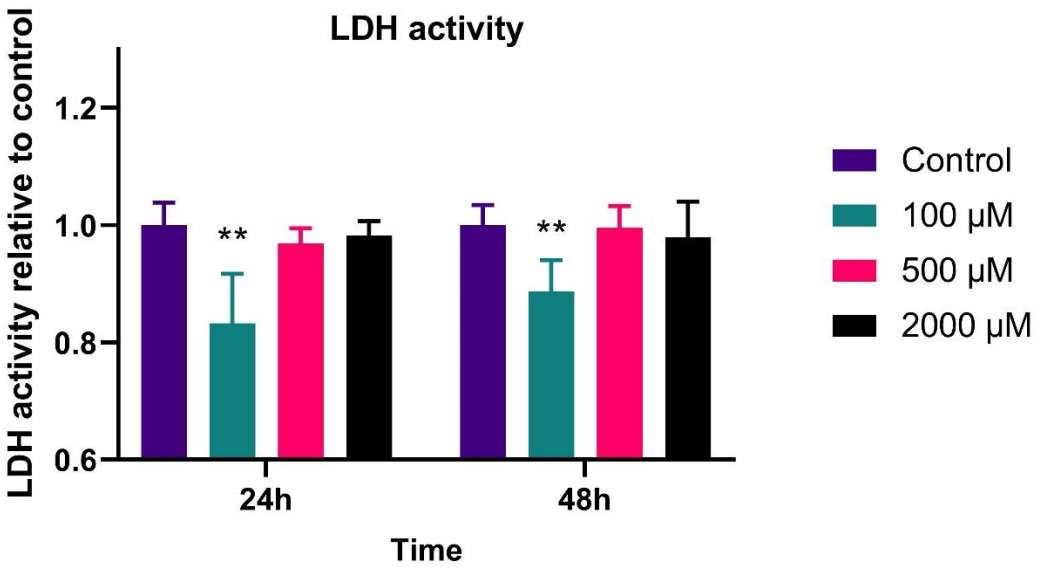

Figure 4.1: Cell toxicity of metformin in MLO-Y4 osteocytes measured by LDH release. *A LDH activity assay was performed in MLO-Y4 osteocytes stimulated with metformin in three doses for 24 and 48 hours. The reported values are means compared to control ± SEM, and are representative of three independent experiments (n=3). Each condition is analyzed in replicates of four. Metformin-treated cells are compared to non-treated cells. Results are considered statistically significant when $p<0.05$ (*). $p<0.01$(**).*

4.2 Metformin-stimulation dose-dependently regulate proliferation of MLO-Y4

Previous studies on osteoblastic cell lines have provided insight into the proliferative effect of metformin on osteoblasts, but considering that no studies has assessed osteocyte proliferation after metformin stimulation, we wanted to investigate this using MLO-Y4 osteocytes. To examine this effect, a MTT proliferation assay was performed. MLO-Y4 cells were cultured as described above and the MTT assay was performed after metformin-stimulation (100, 500 and 2000 µM) for 24, 48 and 72h. The absorbances of all samples are compared to untreated control samples and presented as relative to control. Metformin does not affect cellular proliferation in cells treated with 100 µM compared to untreated cells. After 72 hours, cells stimulated with 500 µM metformin showed reduced proliferation ($p<0.05$). Cells stimulated with 2000 µM metformin showed significant ($p<0.01$) reduced proliferation compared to untreated control cells at all time points examined and the greatest effect was observed after 72 hours (Figure 4.2).

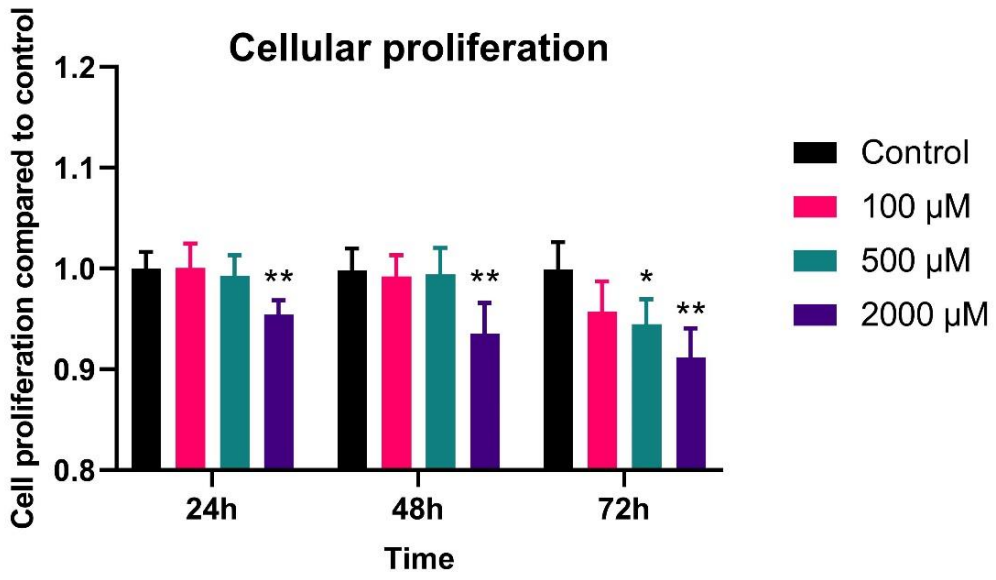

Figure 4.2: MTT proliferation assay in MLO-Y4 osteocytes*. The reported values are means ± SEM, representative of three independent experiments (n=3), with each condition in replicates of five. Metformin-treated cells are compared to untreated cells. Results are considered statistically significant when p<0.05 (*). p<0.01 (**).*

4.3 Metformin does not significantly regulate RANKL and OPG mRNA expression in MLO-Y4 osteocytes

Metformin has previously been demonstrated to activate AMPK in other bone cells and regulate the RANKL/OPG system. Therefore, we wanted to investigate whether metformin can regulate the RANKL/OPG system in MLO-Y4 osteocytes. Cells were stimulated with metformin (100 µM, 500 µM and 2000 µM) for 24, 48 and 72 hours before RNA was isolated and converted to cDNA. mRNA expression for each gene was examined by qPCR in duplicates from three biological replicates and the results are shown in Figure 4.3A and B, presented as relative to the housekeeping gene *GAPDH*. Metformin did not significantly regulate the gene expression of *OPG* and *RANKL* in any of the concentrations and time points. Likewise, there is no statistically significant regulation of the *RANKL/OPG* ratio. However, we can observe that the trend is a dose-dependent decrease of the *RANKL/OPG* ratio compared to the control. (Figure 4.3C).

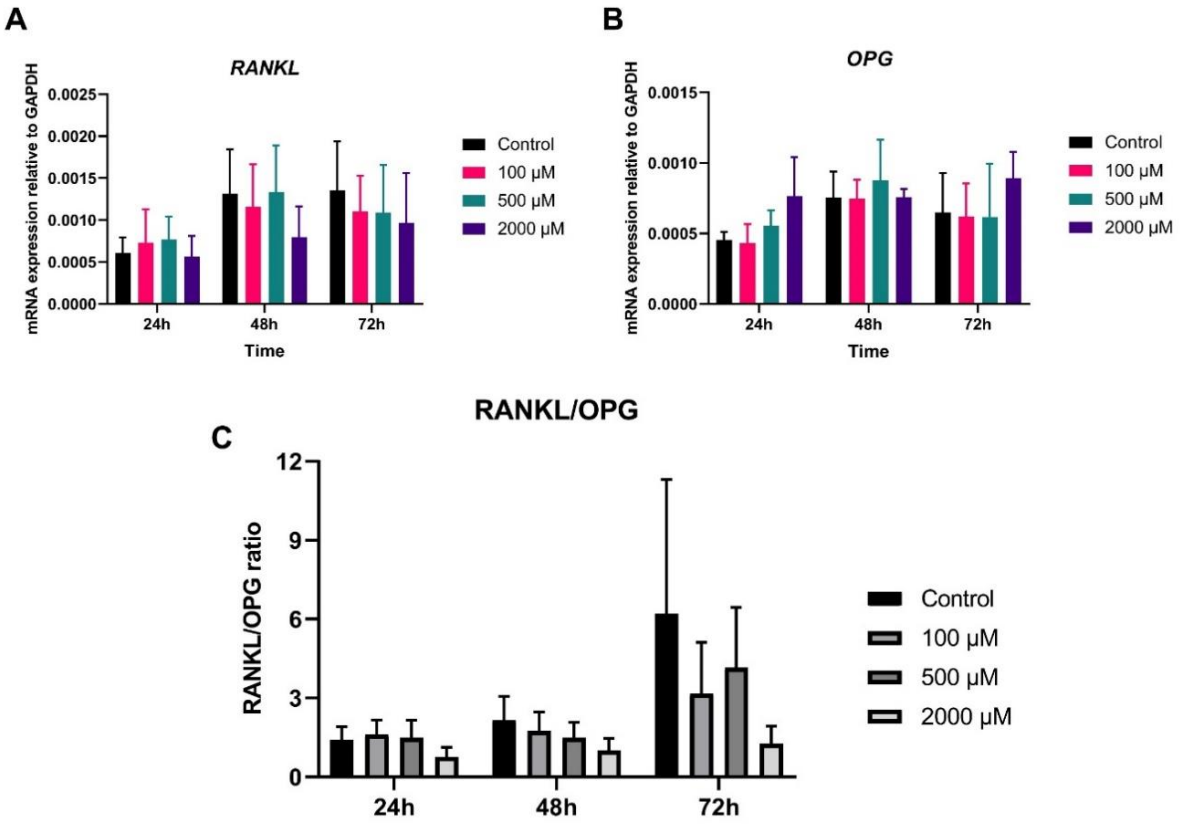

Figure 4.3: RANKL and OPG mRNA expression in metformin-stimulated MLO-Y4 osteocytes*. The effect on mRNA expression of RANKL and OPG examined by qPCR after metformin-stimulation (100 µM, 500 µM and 2000 µM) for 24, 48 and 72 hours. RANKL mRNA expression* ***(A)****, OPG mRNA expression* ***(B)*** *and RANKL/OPG ratio* ***(C)****. The reported values are means ± SEM, representative of three independent experiments (n=3). Each sample is representative of three technical replicates that are pooled and analyzed in duplicate. Relative mRNA expression was calculated with a standard curve method and is relative to GAPDH. Metformin-stimulated cells are compared to control cells. Results are considered statistically significant when p<0.05 (*).*

4.4 Metformin upregulates mRNA expression of the mechanosensitive ion channel *Piezo1*

Furthermore, we wanted to investigate whether the mechanosensitive ion channel Piezo1 is upregulated following metformin stimulation in MLO-Y4 osteocytes, as it is shown to be highly upregulated following mechanical load. *Piezo1* mRNA expression was examined by qPCR after metformin stimulation (100 µM, 500 µM and 2000 µM) as described above, and results are presented in Figure 4.4. There was no significant upregulation of *Piezo1* after metformin stimulation with 100 µM and 500 µM at neither of the time points. *Piezo1* was significantly upregulated compared to the control after 24 hours, but not after 48 and 72 hours. Although not significant, it appears that metformin can give a dose-dependent response in MLO-Y4 cells.

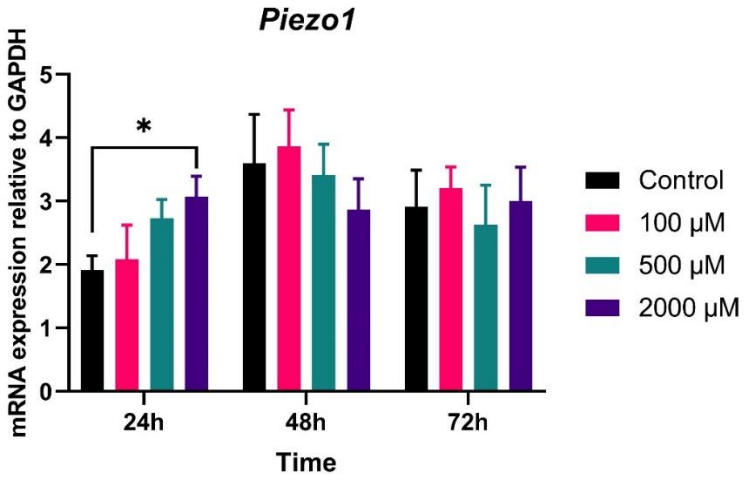

Figure 4.4: Piezo1 mRNA expression in metformin-stimulated MLO-Y4 osteocytes*. The effect of metformin stimulation (100 µM, 500 µM and 2000 µM) on Piezo1 mRNA expression in MLO-Y4 osteocytes examined by qPCR after 24, 48 and 72 hours. The reported values represent means ± SEM, representative of three independent experiments (n=3). Each sample is representative of three technical replicates that are pooled and analyzed in duplicate. Relative mRNA expression was calculated with a standard curve method and is relative to GAPDH. Metformin-stimulated cells are compared to controls. Results are considered statistically significant when p<0.05 (*).*

4.5 mRNA expression of genes in mechanical load induced Wnt signaling are not regulated by metformin in MLO-Y4

Several genes expressed in osteocytes have been shown to be regulated by mechanical load, and therefore we wanted to examine the mRNA regulation of the canonical Wnt/β-catenin signaling pathways ligands *Wnt1*, *Wnt3a* and the Wnt signaling inhibitor *Sost* in MLO-Y4 osteocytes stimulated with metformin. Cells were stimulated with metformin (100 µM, 500 µM and 2000 µM) for 24, 48 and 72 hours and mRNA expression was examined by qPCR. The results show no statistically significant regulation of any of the three genes at any concentration or time point, but all three genes show a tendency to be downregulated dose-dependently after 72 hours (Figure 4.5).

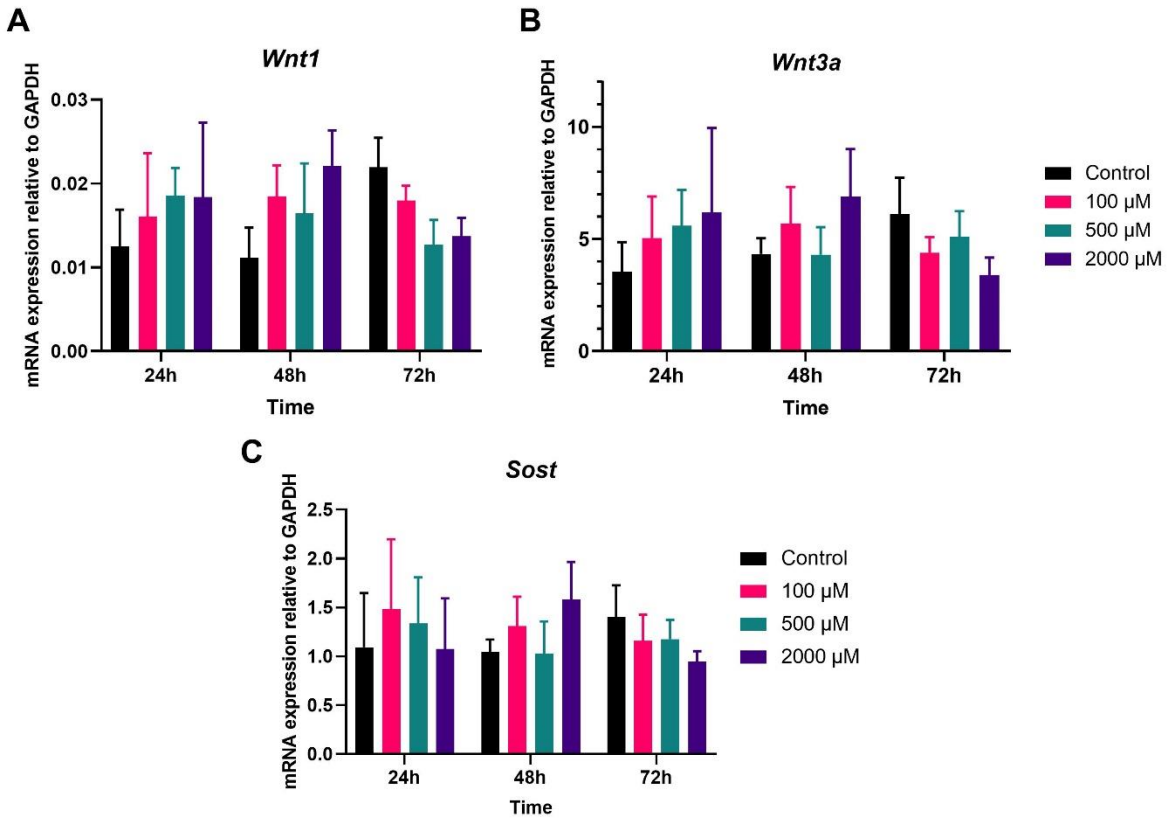

Figure 4.5: Wnt1, Wnt3 and Sost mRNA expression in metformin-stimulated MLO-Y4 osteocytes. *The effect of metformin stimulation (100 µM, 500 µM and 2000 µM) on mRNA expression of genes associated with mechanical load response in MLO-Y4 osteocytes. Wnt1 mRNA expression* ***(A)****, Wnt3a mRNA expression* ***(B)*** *and Sost mRNA expression* ***(C)*** *after 24, 48 and 72 hours. The reported values represent means ± SEM, representative of three independent experiments (n=). Each sample is representative of three technical replicates that are pooled and analyzed in duplicate. Relative mRNA expression was calculated with a standard curve method and sample concentrations are relative to GAPDH. Metformin-stimulated cells are compared to controls. Results are considered statistically significant when p<0.05 (*).*

4.6 Metformin does not stimulate gene and protein expression of mechanical load inducible PGE_2

PGE_2 release is considered a hallmark of the mechanical load response in osteocytes, and therefore we wanted to investigate whether metformin stimulates mRNA expression of the gene *Ptgs2*, which encodes the enzyme necessary for PGE_2 synthesis. Furthermore, we wanted to investigate PGE_2 secretion at protein level. *Ptgs2* mRNA expression was examined by qPCR as described above. Metformin did not significantly regulate mRNA expression of *Ptgs2* at any time points (Figure 4.6).

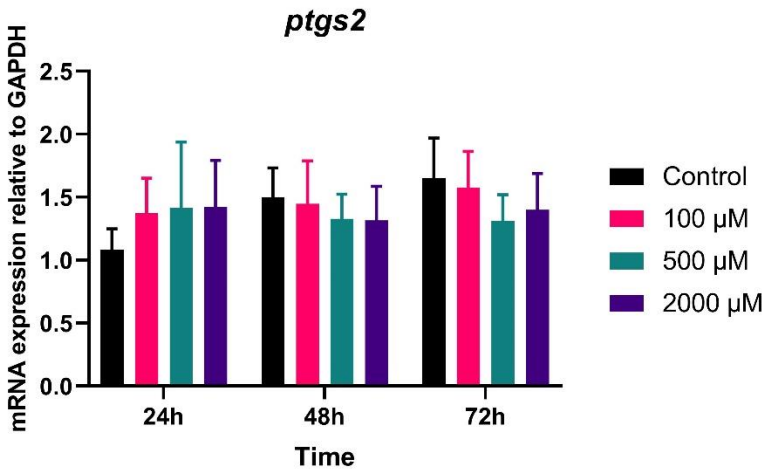

Figure 4.6: Ptgs2 mRNA expression in metformin-stimulated MLO-Y4 osteocytes. *Mechanical load inducible Ptgs2 mRNA expression was examined by qPCR in MLO-Y4 cells after metformin stimulation (100 µM, 500 µM and 2000 µM) after 24, 48 and 72 hours. The reported values represent means ± SEM, representative of three independent experiments (n=3). Each sample is representative of three technical replicates that are pooled and analyzed in duplicate. Relative mRNA expression was calculated with a standard curve method and is relative to GAPDH. Metformin-stimulated cells are compared to controls. Results are considered statistically significant when p<0.05 (*).*

Furthermore, medium from cells stimulated with metformin (100 µM, 500 µM and 2000 µM) was collected after 24, 48 and 72 hours, and PGE_2 protein secretion was studied by the use of a monoclonal ELISA PGE_2 kit. There was no upregulation of PGE_2 after metformin stimulation. In contrast, PGE_2 protein secretion appeared to be lower compared to control after 72 hours (Figure 4.7). Statistics are not performed due to lack of a third biological replicate, so no conclusions can be made from the protein analysis.

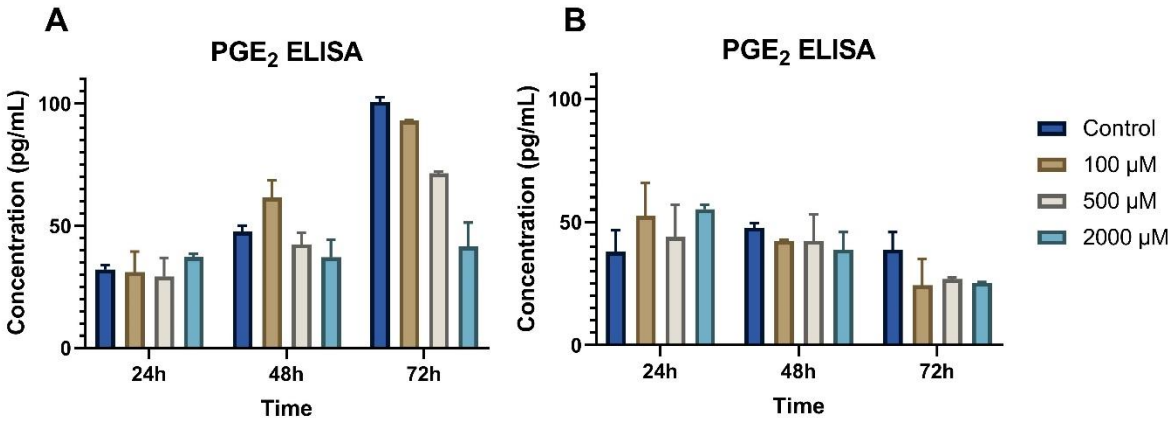

Figure 4.7: PGE_2 protein secretion examined by ELISA. *Medium from MLO-Y4 cells stimulated with metformin (100 µM, 500 µM and 2000 µM) was collected after 24, 48 and 72 hours. Graphs **A** and **B** each represent one biological replicate (n=2). The reported values are means ±SD with each sample analyzed in duplicate and each sample is representative of three technical replicates.*

4.7 Metformin reduces apoptotic cell death following radiation treatment

Earlier studies have shown that cell viability is decreased in irradiated MLO-Y4 cells and that apoptosis is increased dependent on the radiation dose (75). Thus, irradiation damage osteocyte viability and therefore, it was of interest to investigate whether metformin could protect against RT-induced apoptosis. Metformin-stimulated (100 µM, 500 µM and 2000 µM) cells were irradiated with a dose of 5 Gy and compared to non-irradiated cells stimulated with metformin after 24 and 48 hours after radiation. The extent of apoptosis was measured with a cell death detection kit based on a sandwich ELISA assay. At both 24 and 48 hours, osteocyte apoptosis was greater in the irradiated cells than in the control cells (0 Gy). After 24 hours, we observed a slight decrease in apoptosis in the metformin-stimulated cells compared to the control in the cells exposed to 5 Gy radiation. After 48 hours, the decreased rate of apoptosis appeared to be dose-dependent, with a greater decrease of apoptosis in metformin-stimulated cells compared to control than after 24 hours (Figure 4.8). Statistics were not performed due to lack of sufficient biological replicates and no conclusions can be made before the experiment is repeated.

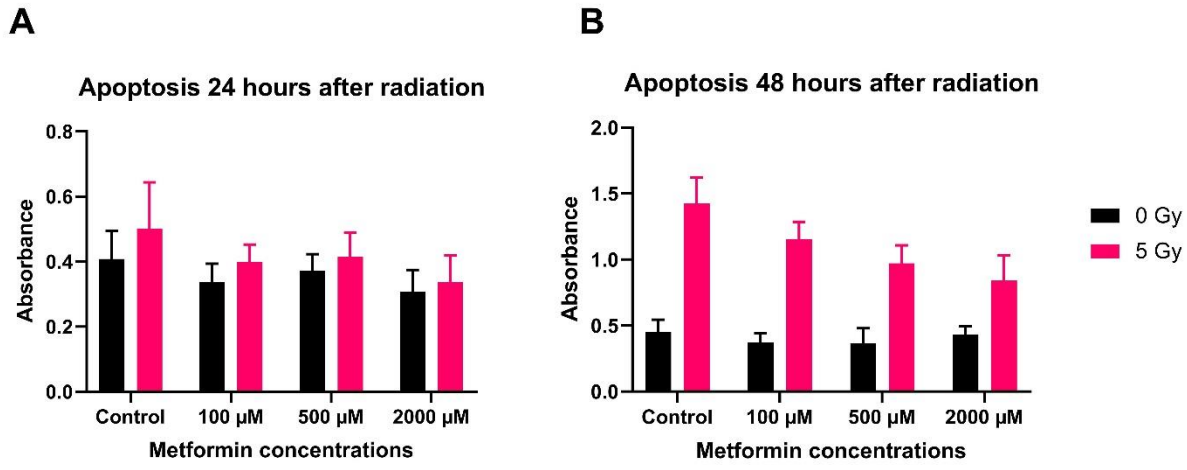

Figure 4.8: Cellular apoptosis of irradiated MLO-Y4 cells stimulated with metformin examined by ELISA cell death detection kit. *Cells were stimulated with metformin (100 µM, 500 µM and 2000 µM) and irradiated with 5 Gy. Apoptosis was measured after 24 and 48 hours of radiation of both irradiated cells and control cells. The reported values represent means ± SD from one biological replicate with five technical replicates (n=1). Metformin-stimulated cells were compared to controls.*

5. Discussion

Osteoporosis is a skeletal disease that constitutes a major health concern due to the associated fragility fractures. Whereas several pharmacological treatment options are available, exercise is regarded as an important countermeasure against osteoporosis development. Upon exercise, AMPK is activated in cells due to the lack of cellular energy. Recently, metformin has gained attention for its role as an AMPK activator and has been suggested that metformin may act as an exercise mimetic in bone and thus play beneficial roles in bone physiology and disease. Considering most research on metformin and bone has been focused on bone progenitor cells and osteoblasts, there are limited information whether metformin affects osteocytes. The murine osteocyte-like MLO-Y4 cell line was chosen because it is shown to respond rapidly to fluid flow, which makes it suitable to compare metformin stimulation with fluid flow response. MLO-Y4 cells have a dendritic morphology and an osteocytic phenotype with low expression of ALP, whereas the expression of osteocalcin, E11 and Cx43 is high. Moreover, the cells have been shown to be useful in the study of cell death and apoptosis (132).

We found that metformin in the given concentrations does not cause cytotoxic effects measured by LDH release in MLO-Y4 cells after 24 and 48 hours. If metformin in any of the given concentrations have shown to significantly increase LDH activity and thus cause cytotoxicity, this concentration would have been excluded for the remaining experiments. Unexpectedly, metformin significantly reduced cytotoxic damage in MLO-Y4 osteocytes at lower concentrations (100 µM) compared to control. It is difficult to explain the reduced LDH release in this concentration without further experiments, but one might assume that metformin could have beneficial protective effects on cell viability in lower doses. No studies have previously studied the cytotoxic potential of metformin in osteocytes and there are few studies regarding metformin and cytotoxicity in other bone cells. A previous study in bone marrow mesenchymal stem cells (BMSCs) have demonstrated dose-dependent cytotoxic damage after metformin stimulation in doses of 5 and 10 mM, but no cytotoxicity when stimulated with 1 mM (133). This study is not directly comparable to ours as it was performed in stem cells, but since osteocytes descend from BMSCs, some mechanisms could be similar.

Previously, Shah et al. reported that metformin does not affect osteoblastic proliferation in doses up to 500 µM after 24 hours, whereas other studies on osteoblastic cells show increased proliferation after stimulation with metformin in doses ranging from 10-500 µM (93, 103, 106). A recent study by Mu et al. examined the proliferative activity of murine pre-osteoblasts stimulated with metformin (300-1200 µM) by MTT and found increased proliferation in high

glucose cells stimulated with doses ≥600 µM metformin (134). Our results showed no effect of low doses of metformin on MLO-Y4 cell proliferation, but decreased proliferation with 2000 µM, which is in line with what Shah et al. reported, but in contrast to studies reporting increased proliferative capacity of osteoblasts stimulated with metformin. As most studies are performed in BMPCs and osteoblasts, they are not fully comparable to our results. Additionally, few studies have investigated the effect of metformin on proliferation in doses up to 2000 µM where we observed inhibition of proliferation. One study reported decreased proliferation in two human stem cell-like osteosarcoma cell lines stimulated with metformin (0.1-5 mM) in doses ≥ 1 mM after 48 hours measured by MTT (135), in accordance with our results.

One possible explanation for why metformin can inhibit proliferation is through the actions of AMPK, which has been shown to induce cell cycle arrest and inhibit cellular proliferation in several cell types through mTOR inhibition, both in malignant and non-malignant cells (136). Therefore, metformin might decrease the proliferative activity of the osteocytes in favor of conserving cellular energy. Another possible explanation is that cells treated with high doses of metformin (2000 µM) in fact have less favorable conditions to thrive and proliferate, but without causing increased cytotoxic effects through LDH release. Considering mature osteocytes are terminally differentiated cells and MLO-Y4 are highly proliferative, the results cannot be expected to apply to mature osteocytes in vivo. MLO-Y4 is a cell line of less differentiated osteocytes, and thus have the capacity to proliferate in culture. Additionally, MLO-Y4 cells are murine cells that are not directly comparable to human cells due to species differences.

Mechanical load is known to inhibit osteoclastogenesis and also to activate AMPK. Studies have shown that pulsatile fluid flow in MLO-Y4 cells reduced the *RANKL*/*OPG* ratio at the mRNA level (both *RANKL* and *OPG* upregulation) after 2 hours, but that this effect was reversed at 24 and 48 hours (137). Since we hypothesized that metformin acts as a mechanical load mimetic, we wanted to examine whether there is a similar response to metformin as to mechanical load. Previous studies in osteoblasts have demonstrated that metformin reduces *RANKL* mRNA expression and increases *OPG* mRNA expression (116). No studies have investigated the effect of metformin on *RANKL* and *OPG* mRNA expression in osteocytes, but one study reported that the AMPK activator AICAR significantly decreased *RANKL* dose- and time dependently, whereas *OPG* was not significantly upregulated. In their study, the RANKL/OPG ratio demonstrated a significant dose-dependent decrease in response to metformin (138). In our study, neither *OPG* nor *RANKL* showed significant regulation in any

concentrations. Nevertheless, the RANKL/OPG ratio appear to have a dose-dependent decrease, but as it is not statistically significant, we cannot be certain of this effect. RANKL and OPG are important mediators in osteoclastogenesis. A decrease in the RANKL/OPG ratio indicates decreased bone resorption due to reduced osteoclast differentiation and activity. This effect would be beneficial considering the potential of metformin as an osteoporotic therapy. A weakness of our study is that we did not examine gene or protein expression after 2 hours of metformin stimulation, and that we therefore might miss immediate effects caused by metformin. Furthermore, our results on *RANKL* and *OPG* mRNA expression varied greatly between the biological replicates. If we study the biological replicates independently, the common pattern for all is a considerable decrease in the RANKL/OPG ratio at the highest concentration (2000 µM) at all time points compared to the control (Appendix 5). This is in line with the results of Yokomoto-Umakoshi et al. that reported a decreased RANKL/OPG ratio after 0.5 mM and 1 mM AICAR stimulation (138). AICAR is a AMP mimetic and activates AMPK directly, whereas metformin might be a less specific activator of AMPK as it mainly acts to increase AMP/ATP ratio, and thus require higher doses to yield similar effects. In addition, metformin have AMPK-independent effects and can act through different pathways. Although metformin does not seem to mimic the effects of mechanical load in the case of *RANKL* and *OPG*, both mechancial load and metformin tend to decrease the RANKL/OPG ratio, which will exert an inhibitory effect on osteoclastogenesis.

The mechanosensitive ion channel Piezo1 has previously been shown to be an important mechanosensor in osteocytes and it is demonstrated that *Piezo1* mRNA expression is highly upregulated following fluid flow shear stress (33). It was of interest to investigate whether metformin can mimic this effect. Our results show that metformin is capable of inducing *Piezo1* mRNA expression in MLO-Y4 osteocytes. Unfortunately, we did not examine the effect shortly after metformin stimulation. In the study by Li et al., mRNA expression was analyzed immediately after fluid flow. Nevertheless, we found a significant increase of *Piezo1* mRNA levels after 24 hours, but not after 42 and 72 hours. This could suggest that upregulation of *Piezo1* is an acute effect of metformin-stimulation, similar to the effect of mechanical load. Whether this effect is AMPK-mediated remains to be investigated. In contrast to Li et al. that reported that administration of the Piezo1 agonist Yoda1 resulted in increased expression of *Ptgs2*, *Wnt1* and *OPG* in MLO-Y4 osteocytes, metformin does not have the same effect to mimic fluid flow via Piezo1. Anyhow, an increase of Piezo1 is shown to enhance bone formation. The importance of Piezo1 as a mechanosensor is highlighted by recent studies that reported that Piezo1 deficiency results in osteoporosis due to lack of mechanosensation and

transduction in osteoblastic cells and therefore decreases bone formation and increase bone resorption by osteoclasts (33, 139, 140).

Upon mechanical load, the expression of several Wnt signaling genes are induced in osteocytes. Wnt1 and Wnt3a are typical ligands in the canonical Wnt/β-catenin signaling pathway and are known to be involved in the bone response to mechanical load. Santos et al. has reported an increased expression of *Wnt3a* in MLO-Y4 osteocytes 3 hours following pulsatile fluid flow, later confirmed by Huang et al. that in addition reported upregulation of *Wnt1*, both after 2 hours. The latter study found after 24 and 48 hours, this effect was blunted (55, 141). These findings suggest that in vitro, osteocytes respond to mechanical load through modulating mRNA levels of *Wnt1* and *Wnt3a*. Considering the fact that we did not study mRNA expression shortly after metformin stimulation, this potential effect may have been missed. Our results show no significant regulation after 24, 48 and 72 hours, which is in line with the results of these studies. To our knowledge, no studies have investigated the effect of metformin and Wnt ligand expression in any type of bone cells. However, several studies have investigated other parts of the Wnt signaling pathway in osteoblastic cells, and found that metformin, through AMPK-dependent mechanisms, increase Wnt signaling and osteoblastic differentiation through stabilization of β-catenin (110, 142).

Sost, which encodes the Wnt signaling pathway inhibitor sclerostin, has been shown to be downregulated in osteocytes in response to mechanical load. Downregulation of the Wnt signaling inhibitor leads to increased bone formation through increased Wnt signaling that promotes osteoblastogenesis. A previous study on MLO-Y4 osteocytes demonstrated an increased gene expression of *Sost* that peaked after 24 hours when the cells were stimulated with the AMPK activator AICAR (138). They found that this increase was due to inhibition of the mevalonate pathway through AMPK activation. In contrast to this study, we did not find any significant regulation of *Sost* mRNA levels following metformin-stimulation. This may indicate that metformin is a weaker activator of AMPK, or that metformin acts through other AMPK-independent mechanisms.

As stimulation of PGE_2 secretion is a hallmark of mechanical load response and important in the balance of bone remodeling, we hypothesized that metformin could stimulate *Ptgs2* mRNA expression and PGE_2 protein secretion. Previous studies have shown that fluid flow increase the release of the signaling molecule PGE_2 in MLO-Y4 osteocytes within minutes. In addition, *Ptgs2* mRNA expression was induced shortly after fluid flow and was still evident after 24 hours (143). Although no definite conclusions can be made due to the lack of sufficient

biological replicates, our results do not indicate any upregulation of either Ptgs2 mRNA levels or PGE_2 protein secretion, thus it appears that our hypothesis was incorrect. Considering PGE_2 release is considered an acute effect of fluid flow, it would have been of interest to investigate PGE_2 protein release as well as *Ptgs2* mRNA levels hours after metformin stimulation. It is highly probable that metformin does not mimic this effect of mechanical load in MLO-Y4 osteocytes. In contrast, metformin appears to decrease PGE_2 release dose-dependently after 72 hours. Studies in other cell types outside bone have reported that metformin decreases *Ptgs2* mRNA expression and PGE_2 release dose-dependently, possibly via AMPK-dependent actions (144-146).

Finally, we investigated whether metformin could prevent RT-induced apoptosis in MLO-Y4 osteocytes after 5 Gy ionizing radiation. This dose was chosen because previous studies have shown negative effects on cell viability in MLO-Y4 cells at this dose. Moreover, this dose is relevant to standard doses used for conventional radiation therapy, which is approximately 2 Gy per fraction (75, 147). Previously, osteocytes was shown to be more radiosensitive than osteoblasts (71). It is known that ionizing radiation damages DNA and induces apoptosis in cells, and that this is an early effect of radiation. Additionally, ionizing radiation causes later effects such as continuous production of ROS and induces an inflammatory response (148). Recently, He et al. reported induction of apoptosis of MLO-Y4 osteocytes after only 4 Gy ionizing radiation (75). Our results in are in line with this, showing increased apoptosis in irradiated cells (5 Gy) compared to controls.

Studies in other non-cancer cell types have shown a protective effect of metformin on RT-induced DNA damage (149). It has been reported by several studies that metformin is associated with protective effects against oxidative stress and DNA damage caused by ionizing radiation, by decreasing endogenous ROS generation and enhancement of DNA repair processes. Both these effects are thought to act via AMPK-dependent mechanisms (148, 150). Our results indicate that cells stimulated with metformin appear to dose-dependently protect against apoptosis, shown by the use of a DNA and histone fragmentation ELISA kit. The extent of apoptosis did not appear to be regulated by metformin in cells not exposed to radiation. Considering only one replicate was performed, no conclusions can be made at this point. If metformin is shown to decrease apoptosis in osteocytes following radiation, the drug could have preventive effects on RT-induced osteoporosis. This because osteocyte apoptosis is an initiator of bone remodeling, and accelerated bone remodeling is associated with net bone loss and osteoporosis.

6. Conclusion and future perspectives

Our results have established that metformin is not cytotoxic to MLO-Y4 osteocytes through LDH release, but decreases the rate of proliferation in high doses. Metformin does not significantly regulate *Wnt1*, *Wnt3a*, *Sost*, *Ptgs2*, *OPG* or *RANKL* mRNA expression or PGE_2 protein secretion in any concentrations after 24, 48 or 72 hours in contrast to what is seen after mechanical load. However, metformin seem to lower the RANKL/OPG ratio, which is known to decrease osteoclastogenesis. Moreover, metformin significantly upregulated *Piezo1* mRNA levels in a dose-dependent matter after 24 hours. Upregulation of Piezo1 is associated with increased mechanosensation and subsequent enhanced bone formation. In conclusion, our results cannot confirm that metformin act as a direct mechanical load mimetic through AMPK activation. However, metformin appear to share some similarities to mechanical load, through upregulated Piezo1 and lowered RANKL/OPG ratio that are associated with increased bone formation and decreased bone resorption, respectively. This would indicate a positive effect on bone mass, but would need to be confirmed. Further experiments on metformin and osteocytes are needed, and acute effects after a short stimulation (approximately 2-3 hours) with metformin should also be included. In the future, it would also be of interest to investigate the possible combined effect of metformin and fluid flow on osteocyte gene expression in vitro.

Our preliminary experiments on metformin and ionizing radiation showed promising results regarding prevention of RT-induced apoptosis by metformin. Our results indicate that metformin decreases apoptosis in a dose- and time-dependent manner in irradiated MLO-Y4 osteocytes. Considering osteocyte apoptosis is an initiator of accelerated bone remodeling and bone loss, prevention of apoptosis by metformin could possibly reduce bone loss in cancer patients subjected to radiation therapy. In the future, our results regarding the protective effects of metformin on apoptosis of irradiated MLO-Y4 osteocytes will need to be confirmed and molecular mechanisms should be investigated more in detail.

7. References

1. Datta HK, Ng WF, Walker JA, Tuck SP, Varanasi SS. The cell biology of bone metabolism. Journal of Clinical Pathology. 2008;61(5):577-87.
2. Florencio-Silva R, Sasso GRdS, Sasso-Cerri E, Simões MJ, Cerri PS. Biology of Bone Tissue: Structure, Function, and Factors That Influence Bone Cells. Biomed Res Int. 2015;2015:421746-.
3. Han Y, You X, Xing W, Zhang Z, Zou W. Paracrine and endocrine actions of bone—the functions of secretory proteins from osteoblasts, osteocytes, and osteoclasts. Bone Research. 2018;6(1):16.
4. Downey PA, Siegel MI. Bone Biology and the Clinical Implications for Osteoporosis. Physical Therapy. 2006;86(1):77-91.
5. Bala Y, Zebaze R, Seeman E. Role of cortical bone in bone fragility. Current Opinion in Rheumatology. 2015;27(4):406-13.
6. Morgan EF, Barnes GL, Einhorn TA. Chapter 1 - The Bone Organ System: Form and Function. In: Marcus R, Feldman D, Dempster DW, Luckey M, Cauley JA, editors. Osteoporosis (Fourth Edition). San Diego: Academic Press; 2013. p. 3-20.
7. Oftadeh R, Perez-Viloria M, Villa-Camacho JC, Vaziri A, Nazarian A. Biomechanics and mechanobiology of trabecular bone: a review. J Biomech Eng. 2015;137(1):0108021-01080215.
8. Fonseca H, Moreira-Gonçalves D, Coriolano H-JA, Duarte JA. Bone quality: the determinants of bone strength and fragility. Sports Med. 2014;44(1):37-53.
9. Teitelbaum SL. Bone resorption by osteoclasts. Science (New York, NY). 2000;289(5484):1504-8.
10. Kim JH, Kim N. Signaling Pathways in Osteoclast Differentiation. Chonnam Med J. 2016;52(1):12-7.
11. Kong Y-Y, Yoshida H, Sarosi I, Tan H-L, Timms E, Capparelli C, et al. OPGL is a key regulator of osteoclastogenesis, lymphocyte development and lymph-node organogenesis. Nature. 1999;397(6717):315-23.
12. Mizuno A, Kanno T, Hoshi M, Shibata O, Yano K, Fujise N, et al. Transgenic mice overexpressing soluble osteoclast differentiation factor (sODF) exhibit severe osteoporosis. Journal of bone and mineral metabolism. 2002;20:337-44.
13. Theoleyre S, Wittrant Y, Tat SK, Fortun Y, Redini F, Heymann D. The molecular triad OPG/RANK/RANKL: involvement in the orchestration of pathophysiological bone remodeling. Cytokine & growth factor reviews. 2004;15(6):457-75.
14. Capulli M, Paone R, Rucci N. Osteoblast and osteocyte: games without frontiers. Arch Biochem Biophys. 2014;561:3-12.
15. Vimalraj S, Arumugam B, Miranda PJ, Selvamurugan N. Runx2: Structure, function, and phosphorylation in osteoblast differentiation. Int J Biol Macromol. 2015;78:202-8.
16. Gaur T, Lengner CJ, Hovhannisyan H, Bhat RA, Bodine PVN, Komm BS, et al. Canonical WNT signaling promotes osteogenesis by directly stimulating Runx2 gene expression. The Journal of biological chemistry. 2005;280(39):33132-40.
17. Nakashima K, Zhou X, Kunkel G, Zhang Z, Deng JM, Behringer RR, et al. The novel zinc finger-containing transcription factor osterix is required for osteoblast differentiation and bone formation. Cell. 2002;108(1):17-29.
18. Anderson HC. Molecular biology of matrix vesicles. Clin Orthop Relat Res. 1995(314):266-80.
19. Manolagas SC. Birth and Death of Bone Cells: Basic Regulatory Mechanisms and Implications for the Pathogenesis and Treatment of Osteoporosis*. Endocrine reviews. 2000;21(2):115-37.

20. Mullen CA, Haugh MG, Schaffler MB, Majeska RJ, McNamara LM. Osteocyte differentiation is regulated by extracellular matrix stiffness and intercellular separation. Journal of the Mechanical Behavior of Biomedical Materials. 2013;28:183-94.
21. Brotto M, Bonewald L. Bone and muscle: Interactions beyond mechanical. Bone. 2015;80:109-14.
22. Bonewald LF. The amazing osteocyte. Journal of bone and mineral research : the official journal of the American Society for Bone and Mineral Research. 2011;26(2):229-38.
23. Goldring SR. The osteocyte: key player in regulating bone turnover. RMD Open. 2015;1(Suppl 1):e000049-e.
24. Tagliaferri C, Wittrant Y, Davicco M-J, Walrand S, Coxam V. Muscle and bone, two interconnected tissues. Ageing Res Rev. 2015;21:55-70.
25. Schaffler MB, Cheung WY, Majeska R, Kennedy O. Osteocytes: master orchestrators of bone. Calcif Tissue Int. 2014;94(1):5-24.
26. Franz-Odendaal TA, Hall BK, Witten PE. Buried alive: how osteoblasts become osteocytes. Dev Dyn. 2006;235(1):176-90.
27. Zhang K, Barragan-Adjemian C, Ye L, Kotha S, Dallas M, Lu Y, et al. E11/gp38 selective expression in osteocytes: regulation by mechanical strain and role in dendrite elongation. Mol Cell Biol. 2006;26(12):4539-52.
28. Dallas SL, Prideaux M, Bonewald LF. The osteocyte: an endocrine cell ... and more. Endocrine reviews. 2013;34(5):658-90.
29. Tiede-Lewis LM, Dallas SL. Changes in the osteocyte lacunocanalicular network with aging. Bone. 2019;122:101-13.
30. Hung CT, Pollack SR, Reilly TM, Brighton CT. Real-time calcium response of cultured bone cells to fluid flow. Clin Orthop Relat Res. 1995(313):256-69.
31. Lu XL, Huo B, Park M, Guo XE. Calcium response in osteocytic networks under steady and oscillatory fluid flow. Bone. 2012;51(3):466-73.
32. Botello-Smith WM, Jiang W, Zhang H, Ozkan AD, Lin Y-C, Pham CN, et al. A mechanism for the activation of the mechanosensitive Piezo1 channel by the small molecule Yoda1. Nature Communications. 2019;10(1):4503.
33. Li X, Han L, Nookaew I, Mannen E, Silva MJ, Almeida M, et al. Stimulation of Piezo1 by mechanical signals promotes bone anabolism. Elife. 2019;8.
34. Bivi N, Condon KW, Allen MR, Farlow N, Passeri G, Brun LR, et al. Cell autonomous requirement of connexin 43 for osteocyte survival: consequences for endocortical resorption and periosteal bone formation. Journal of bone and mineral research : the official journal of the American Society for Bone and Mineral Research. 2012;27(2):374-89.
35. Davis HM, Aref MW, Aguilar-Perez A, Pacheco-Costa R, Allen K, Valdez S, et al. Cx43 overexpression in osteocytes prevents osteocyte apoptosis and preserves cortical bone quality in aging mice. JBMR Plus. 2018;2(4):206-16.
36. Xia X, Batra N, Shi Q, Bonewald LF, Sprague E, Jiang JX. Prostaglandin promotion of osteocyte gap junction function through transcriptional regulation of connexin 43 by glycogen synthase kinase 3/beta-catenin signaling. Mol Cell Biol. 2010;30(1):206-19.
37. Park JY, Pillinger MH, Abramson SB. Prostaglandin E2 synthesis and secretion: The role of PGE2 synthases. Clinical Immunology. 2006;119(3):229-40.
38. Blackwell KA, Raisz LG, Pilbeam CC. Prostaglandins in bone: bad cop, good cop? Trends in Endocrinology & Metabolism. 2010;21(5):294-301.
39. Choudhary S, Pilbeam C. Prostaglandins and bone metabolism. Principles of Bone Biology: Elsevier; 2020. p. 1247-69.
40. Komiya Y, Habas R. Wnt signal transduction pathways. Organogenesis. 2008;4(2):68-75.

41. Steinhart Z, Angers S. Wnt signaling in development and tissue homeostasis. Development. 2018;145(11):dev146589.
42. Bonewald LF, Johnson ML. Osteocytes, mechanosensing and Wnt signaling. Bone. 2008;42(4):606-15.
43. Semenov M, Tamai K, He X. SOST is a ligand for Lrp5/Lrp6 and a Wnt signaling inhibitor. The Journal of biological chemistry. 2005;280:26770-5.
44. Li X, Ominsky MS, Niu Q-T, Sun N, Daugherty B, D'Agostin D, et al. Targeted Deletion of the Sclerostin Gene in Mice Results in Increased Bone Formation and Bone Strength. Journal of Bone and Mineral Research. 2008;23(6):860-9.
45. Glinka A, Wu W, Delius H, Monaghan AP, Blumenstock C, Niehrs C. Dickkopf-1 is a member of a new family of secreted proteins and functions in head induction. Nature. 1998;391(6665):357-62.
46. Plotkin LI. Apoptotic osteocytes and the control of targeted bone resorption. Curr Osteoporos Rep. 2014;12(1):121-6.
47. Langdahl B, Ferrari S, Dempster DW. Bone modeling and remodeling: potential as therapeutic targets for the treatment of osteoporosis. Ther Adv Musculoskelet Dis. 2016;8(6):225-35.
48. Raggatt LJ, Partridge NC. Cellular and molecular mechanisms of bone remodeling. The Journal of biological chemistry. 2010;285(33):25103-8.
49. Hadjidakis DJ, Androulakis II. Bone remodeling. Ann N Y Acad Sci. 2006;1092:385-96.
50. Kenkre JS, Bassett J. The bone remodelling cycle. Ann Clin Biochem. 2018;55(3):308-27.
51. Eriksen EF. Cellular mechanisms of bone remodeling. Rev Endocr Metab Disord. 2010;11(4):219-27.
52. Kennedy OD, Herman BC, Laudier DM, Majeska RJ, Sun HB, Schaffler MB. Activation of resorption in fatigue-loaded bone involves both apoptosis and active pro-osteoclastogenic signaling by distinct osteocyte populations. Bone. 2012;50(5):1115-22.
53. Jilka RL, Noble B, Weinstein RS. Osteocyte apoptosis. Bone. 2013;54(2):264-71.
54. Al-Dujaili SA, Lau E, Al-Dujaili H, Tsang K, Guenther A, You L. Apoptotic osteocytes regulate osteoclast precursor recruitment and differentiation in vitro. Journal of cellular biochemistry. 2011;112(9):2412-23.
55. Santos A, Bakker AD, Zandieh-Doulabi B, Semeins CM, Klein-Nulend J. Pulsating fluid flow modulates gene expression of proteins involved in Wnt signaling pathways in osteocytes. J Orthop Res. 2009;27(10):1280-7.
56. Robling AG, Niziolek PJ, Baldridge LA, Condon KW, Allen MR, Alam I, et al. Mechanical stimulation of bone in vivo reduces osteocyte expression of Sost/sclerostin. The Journal of biological chemistry. 2008;283(9):5866-75.
57. Tu X, Rhee Y, Condon KW, Bivi N, Allen MR, Dwyer D, et al. Sost downregulation and local Wnt signaling are required for the osteogenic response to mechanical loading. Bone. 2012;50(1):209-17.
58. Compston JE, McClung MR, Leslie WD. Osteoporosis. The Lancet. 2019;393(10169):364-76.
59. Cooper C, Cole ZA, Holroyd CR, Earl SC, Harvey NC, Dennison EM, et al. Secular trends in the incidence of hip and other osteoporotic fractures. Osteoporos Int. 2011;22(5):1277-88.
60. Rachner TD, Khosla S, Hofbauer LC. Osteoporosis: now and the future. Lancet (London, England). 2011;377(9773):1276-87.
61. Khosla S, Oursler MJ, Monroe DG. Estrogen and the skeleton. Trends Endocrinol Metab. 2012;23(11):576-81.

62. Drake MT, Clarke BL, Lewiecki EM. The Pathophysiology and Treatment of Osteoporosis. Clin Ther. 2015;37(8):1837-50.
63. Duque G, Troen BR. Understanding the Mechanisms of Senile Osteoporosis: New Facts for a Major Geriatric Syndrome. Journal of the American Geriatrics Society. 2008;56(5):935-41.
64. Raisz LG. Pathogenesis of osteoporosis: concepts, conflicts, and prospects. The Journal of clinical investigation. 2005;115(12):3318-25.
65. Bergmann P, Body JJ, Boonen S, Boutsen Y, Devogelaer JP, Goemaere S, et al. Loading and skeletal development and maintenance. J Osteoporos. 2010;2011:786752.
66. Bassey EJ, Rothwell MC, Littlewood JJ, Pye DW. Pre- and postmenopausal women have different bone mineral density responses to the same high-impact exercise. Journal of bone and mineral research : the official journal of the American Society for Bone and Mineral Research. 1998;13(12):1805-13.
67. Kohrt WM, Bloomfield SA, Little KD, Nelson ME, Yingling VR. American College of Sports Medicine Position Stand: physical activity and bone health. Med Sci Sports Exerc. 2004;36(11):1985-96.
68. Sunyecz JA. The use of calcium and vitamin D in the management of osteoporosis. Ther Clin Risk Manag. 2008;4(4):827-36.
69. Baxter NN, Habermann EB, Tepper JE, Durham SB, Virnig BA. Risk of pelvic fractures in older women following pelvic irradiation. Jama. 2005;294(20):2587-93.
70. Kang Y-M, Chao T-F, Wang T-H, Hu Y-W. Increased risk of pelvic fracture after radiotherapy in rectal cancer survivors: A propensity matched study. Cancer Medicine. 2019;8(8):3639-47.
71. Wright LE, Buijs JT, Kim H-S, Coats LE, Scheidler AM, John SK, et al. Single-Limb Irradiation Induces Local and Systemic Bone Loss in a Murine Model. Journal of bone and mineral research : the official journal of the American Society for Bone and Mineral Research. 2015;30(7):1268-79.
72. Kondo H, Searby ND, Mojarrab R, Phillips J, Alwood J, Yumoto K, et al. Total-body irradiation of postpubertal mice with (137)Cs acutely compromises the microarchitecture of cancellous bone and increases osteoclasts. Radiat Res. 2009;171(3):283-9.
73. Bandstra ER, Pecaut MJ, Anderson ER, Willey JS, De Carlo F, Stock SR, et al. Long-term dose response of trabecular bone in mice to proton radiation. Radiat Res. 2008;169(6):607-14.
74. Willey JS, Lloyd SAJ, Nelson GA, Bateman TA. Ionizing Radiation and Bone Loss: Space Exploration and Clinical Therapy Applications. Clinical reviews in bone and mineral metabolism. 2011;9(1):54-62.
75. He F, Bai J, Wang J, Zhai J, Tong L, Zhu G. Irradiation-induced osteocyte damage promotes HMGB1-mediated osteoclastogenesis in vitro. J Cell Physiol. 2019;234(10):17314-25.
76. Chandra A, Lin T, Young T, Tong W, Ma X, Tseng W-J, et al. Suppression of Sclerostin Alleviates Radiation-Induced Bone Loss by Protecting Bone-Forming Cells and Their Progenitors Through Distinct Mechanisms. Journal of bone and mineral research : the official journal of the American Society for Bone and Mineral Research. 2017;32(2):360-72.
77. Li J, Kwong DL, Chan GC. The effects of various irradiation doses on the growth and differentiation of marrow-derived human mesenchymal stromal cells. Pediatr Transplant. 2007;11(4):379-87.
78. D'Oronzo S, Stucci S, Tucci M, Silvestris F. Cancer treatment-induced bone loss (CTIBL): Pathogenesis and clinical implications. Cancer Treatment Reviews. 2015;41(9):798-808.

79. Rodan GA, Fleisch HA. Bisphosphonates: mechanisms of action. The Journal of clinical investigation. 1996;97(12):2692-6.
80. Anagnostis P, Gkekas NK, Potoupnis M, Kenanidis E, Tsiridis E, Goulis DG. New therapeutic targets for osteoporosis. Maturitas. 2019;120:1-6.
81. Jeyabalan J, Shah M, Viollet B, Chenu C. AMP-activated protein kinase pathway and bone metabolism. J Endocrinol. 2012;212(3):277-90.
82. Garcia D, Shaw RJ. AMPK: Mechanisms of Cellular Energy Sensing and Restoration of Metabolic Balance. Mol Cell. 2017;66(6):789-800.
83. McCarthy AD, Cortizo AM, Sedlinsky C. Metformin revisited: Does this regulator of AMP-activated protein kinase secondarily affect bone metabolism and prevent diabetic osteopathy. World journal of diabetes. 2016;7(6):122-33.
84. Steinberg GR, Kemp BE. AMPK in Health and Disease. Physiol Rev. 2009;89(3):1025-78.
85. Ross FA, MacKintosh C, Hardie DG. AMP-activated protein kinase: a cellular energy sensor that comes in 12 flavours. The FEBS Journal. 2016;283(16):2987-3001.
86. Viollet B, Mounier R, Leclerc J, Yazigi A, Foretz M, Andreelli F. Targeting AMP-activated protein kinase as a novel therapeutic approach for the treatment of metabolic disorders. Diabetes & metabolism. 2007;33(6):395-402.
87. Hardie DG, Scott JW, Pan DA, Hudson ER. Management of cellular energy by the AMP-activated protein kinase system. FEBS Letters. 2003;546(1):113-20.
88. Gowans GJ, Hawley SA, Ross FA, Hardie DG. AMP is a true physiological regulator of AMP-activated protein kinase by both allosteric activation and enhancing net phosphorylation. Cell Metab. 2013;18(4):556-66.
89. Hawley SA, Pan DA, Mustard KJ, Ross L, Bain J, Edelman AM, et al. Calmodulin-dependent protein kinase kinase-beta is an alternative upstream kinase for AMP-activated protein kinase. Cell metabolism. 2005;2(1):9-19.
90. Hardie DG, Ross FA, Hawley SA. AMPK: a nutrient and energy sensor that maintains energy homeostasis. Nat Rev Mol Cell Biol. 2012;13(4):251-62.
91. Jeon SM. Regulation and function of AMPK in physiology and diseases. Exp Mol Med. 2016;48(7):e245.
92. Minokoshi Y, Alquier T, Furukawa N, Kim Y-B, Lee A, Xue B, et al. AMP-kinase regulates food intake by responding to hormonal and nutrient signals in the hypothalamus. Nature. 2004;428(6982):569-74.
93. Shah M, Kola B, Bataveljic A, Arnett TR, Viollet B, Saxon L, et al. AMP-activated protein kinase (AMPK) activation regulates in vitro bone formation and bone mass. Bone. 2010;47(2):309-19.
94. Jeyabalan J, Shah M, Viollet B, Roux JP, Chavassieux P, Korbonits M, et al. Mice lacking AMP-activated protein kinase α1 catalytic subunit have increased bone remodelling and modified skeletal responses to hormonal challenges induced by ovariectomy and intermittent PTH treatment. J Endocrinol. 2012;214(3):349-58.
95. Quinn JMW, Tam S, Sims NA, Saleh H, McGregor NE, Poulton IJ, et al. Germline deletion of AMP-activated protein kinase beta subunits reduces bone mass without altering osteoclast differentiation or function. FASEB journal : official publication of the Federation of American Societies for Experimental Biology. 2010;24(1):275-85.
96. Meier C, Schwartz AV, Egger A, Lecka-Czernik B. Effects of diabetes drugs on the skeleton. Bone. 2016;82:93-100.
97. Bahrambeigi S, Yousefi B, Rahimi M, Shafiei-Irannejad V. Metformin; an old antidiabetic drug with new potentials in bone disorders. Biomedicine & Pharmacotherapy. 2019;109:1593-601.

98. Hunter RW, Hughey CC, Lantier L, Sundelin EI, Peggie M, Zeqiraj E, et al. Metformin reduces liver glucose production by inhibition of fructose-1-6-bisphosphatase. Nat Med. 2018;24(9):1395-406.
99. Vestergaard P, Rejnmark L, Mosekilde L. Relative fracture risk in patients with diabetes mellitus, and the impact of insulin and oral antidiabetic medication on relative fracture risk. Diabetologia. 2005;48(7):1292-9.
100. Melton LJ, 3rd, Leibson CL, Achenbach SJ, Therneau TM, Khosla S. Fracture risk in type 2 diabetes: update of a population-based study. Journal of bone and mineral research : the official journal of the American Society for Bone and Mineral Research. 2008;23(8):1334-42.
101. Kahn SE, Haffner SM, Heise MA, Herman WH, Holman RR, Jones NP, et al. Glycemic Durability of Rosiglitazone, Metformin, or Glyburide Monotherapy. New England Journal of Medicine. 2006;355(23):2427-43.
102. Monami M, Cresci B, Colombini A, Pala L, Balzi D, Gori F, et al. Bone Fractures and Hypoglycemic Treatment in Type 2 Diabetic Patients. A case-control study. 2008;31(2):199-203.
103. Cortizo AM, Sedlinsky C, McCarthy AD, Blanco A, Schurman L. Osteogenic actions of the anti-diabetic drug metformin on osteoblasts in culture. European Journal of Pharmacology. 2006;536(1):38-46.
104. Kanazawa I, Yamaguchi T, Yano S, Yamauchi M, Sugimoto T. Metformin enhances the differentiation and mineralization of osteoblastic MC3T3-E1 cells via AMP kinase activation as well as eNOS and BMP-2 expression. Biochemical and Biophysical Research Communications. 2008;375(3):414-9.
105. Jang WG, Kim EJ, Bae I-H, Lee K-N, Kim YD, Kim D-K, et al. Metformin induces osteoblast differentiation via orphan nuclear receptor SHP-mediated transactivation of Runx2. Bone. 2011;48(4):885-93.
106. Zhen D, Chen Y, Tang X. Metformin reverses the deleterious effects of high glucose on osteoblast function. Journal of Diabetes and its Complications. 2010;24(5):334-44.
107. Wang YG, Qu XH, Yang Y, Han XG, Wang L, Qiao H, et al. AMPK promotes osteogenesis and inhibits adipogenesis through AMPK-Gfi1-OPN axis. Cell Signal. 2016;28(9):1270-82.
108. Zhao J, Yue W, Zhu MJ, Sreejayan N, Du M. AMP-activated protein kinase (AMPK) cross-talks with canonical Wnt signaling via phosphorylation of beta-catenin at Ser 552. Biochem Biophys Res Commun. 2010;395(1):146-51.
109. Chava S, Chennakesavulu S, Gayatri BM, Reddy ABM. A novel phosphorylation by AMP-activated kinase regulates RUNX2 from ubiquitination in osteogenesis over adipogenesis. Cell Death & Disease. 2018;9(7):754.
110. Molinuevo MS, Schurman L, McCarthy AD, Cortizo AM, Tolosa MJ, Gangoiti MV, et al. Effect of metformin on bone marrow progenitor cell differentiation: in vivo and in vitro studies. Journal of bone and mineral research : the official journal of the American Society for Bone and Mineral Research. 2010;25(2):211-21.
111. Takada I, Suzawa M, Matsumoto K, Kato S. Suppression of PPAR Transactivation Switches Cell Fate of Bone Marrow Stem Cells from Adipocytes into Osteoblasts. Ann N Y Acad Sci. 2007;1116(1):182-95.
112. Kang S, Bennett CN, Gerin I, Rapp LA, Hankenson KD, Macdougald OA. Wnt signaling stimulates osteoblastogenesis of mesenchymal precursors by suppressing CCAAT/enhancer-binding protein alpha and peroxisome proliferator-activated receptor gamma. The Journal of biological chemistry. 2007;282(19):14515-24.

113. Kasai T, Bandow K, Suzuki H, Chiba N, Kakimoto K, Ohnishi T, et al. Osteoblast differentiation is functionally associated with decreased AMP kinase activity. J Cell Physiol. 2009;221(3):740-9.
114. Lee YS, Kim YS, Lee SY, Kim GH, Kim BJ, Lee SH, et al. AMP kinase acts as a negative regulator of RANKL in the differentiation of osteoclasts. Bone. 2010;47(5):926-37.
115. Gao Y, Li Y, Xue J, Jia Y, Hu J. Effect of the anti-diabetic drug metformin on bone mass in ovariectomized rats. European Journal of Pharmacology. 2010;635(1):231-6.
116. Mai Q-G, Zhang Z-M, Xu S, Lu M, Zhou R-P, Zhao L, et al. Metformin stimulates osteoprotegerin and reduces RANKL expression in osteoblasts and ovariectomized rats. Journal of cellular biochemistry. 2011;112(10):2902-9.
117. Stunes AK, Erben RG, Schüler C, Eriksen EF, Tice M, Vashishth D, et al. Skeletal effects of plyometric exercise and metformin in ovariectomized rats. Bone. 2020;132:115193.
118. Jeyabalan J, Viollet B, Smitham P, Ellis SA, Zaman G, Bardin C, et al. The anti-diabetic drug metformin does not affect bone mass in vivo or fracture healing. Osteoporosis International. 2013;24(10):2659-70.
119. Takeno A, Kanazawa I, Tanaka K-i, Notsu M, Yokomoto M, Yamaguchi T, et al. Activation of AMP-activated protein kinase protects against homocysteine-induced apoptosis of osteocytic MLO-Y4 cells by regulating the expressions of NADPH oxidase 1 (Nox1) and Nox2. Bone. 2015;77:135-41.
120. Bonewald LF. Establishment and characterization of an osteocyte-like cell line, MLO-Y4. Journal of bone and mineral metabolism. 1999;17(1):61-5.
121. Kato Y, Windle JJ, Koop BA, Mundy GR, Bonewald LF. Establishment of an osteocyte-like cell line, MLO-Y4. Journal of bone and mineral research : the official journal of the American Society for Bone and Mineral Research. 1997;12(12):2014-23.
122. Korzeniewski C, Callewaert DM. An enzyme-release assay for natural cytotoxicity. J Immunol Methods. 1983;64(3):313-20.
123. Chan FK-M, Moriwaki K, De Rosa MJ. Detection of necrosis by release of lactate dehydrogenase activity. Methods in molecular biology (Clifton, NJ). 2013;979:65-70.
124. Freeman WM, Walker SJ, Vrana KE. Quantitative RT-PCR: pitfalls and potential. Biotechniques. 1999;26(1):112-25.
125. Arya M, Shergill IS, Williamson M, Gommersall L, Arya N, Patel HRH. Basic principles of real-time quantitative PCR. Expert Review of Molecular Diagnostics. 2005;5(2):209-19.
126. User Bulletin #2 ABI PRISM 7700 Sequence Detection System [Manual]. Thermo Fisher: Applied biosystems; 1997 [updated 2001. Available from: http://tools.thermofisher.com/content/sfs/manuals/cms_040980.pdf.
127. Prostaglandin E2 ELISA kit - monoclonal [Manual]. Ann Arbor (MI), USA: Cayman Chemical Company; 2016 [Available from: https://www.caymanchem.com/pdfs/514010.pdf.
128. Mosmann T. Rapid colorimetric assay for cellular growth and survival: application to proliferation and cytotoxicity assays. J Immunol Methods. 1983;65(1-2):55-63.
129. Riss TL, Moravec RA, Niles AL. Cell Viability assay In: Sittampalam GS, Grossman A, Brimacombe K, Auld D, Austin CP, Baell J, et al., editors. Assay Guidance Manual. Betcheda (MD) Eli Lilly & Company and the National Center for Advancing Translational Sciences; 2013. p. 298.
130. Bourland JD. Chapter 6 - Radiation Oncology Physics. In: Gunderson LL, Tepper JE, editors. Clinical Radiation Oncology (Fourth Edition). Philadelphia: Elsevier; 2016. p. 93-147.e3.
131. Roche. Cell Death Detection ELISA PLUS 10x 2018 [updated August 2018. Available from: https://www.sigmaaldrich.com/content/dam/sigma-aldrich/docs/Roche/Bulletin/1/celldethrobul.pdf.

132. Kalajzic I, Matthews BG, Torreggiani E, Harris MA, Divieti Pajevic P, Harris SE. In vitro and in vivo approaches to study osteocyte biology. Bone. 2013;54(2):296-306.
133. Śmieszek A, Czyrek A, Basinska K, Trynda J, Skaradzińska A, Siudzińska A, et al. Effect of Metformin on Viability, Morphology, and Ultrastructure of Mouse Bone Marrow-Derived Multipotent Mesenchymal Stromal Cells and Balb/3T3 Embryonic Fibroblast Cell Line. Biomed Res Int. 2015;2015:769402-.
134. Mu W, Wang Z, Ma C, Jiang Y, Zhang N, Hu K, et al. Metformin promotes the proliferation and differentiation of murine preosteoblast by regulating the expression of sirt6 and oct4. Pharmacol Res. 2018;129:462-74.
135. Paiva-Oliveira DI, Martins-Neves SR, Abrunhosa AJ, Fontes-Ribeiro C, Gomes CMF. Therapeutic potential of the metabolic modulator Metformin on osteosarcoma cancer stem-like cells. Cancer Chemotherapy and Pharmacology. 2018;81(1):49-63.
136. Motoshima H, Goldstein BJ, Igata M, Araki E. AMPK and cell proliferation--AMPK as a therapeutic target for atherosclerosis and cancer. J Physiol. 2006;574(Pt 1):63-71.
137. You L, Temiyasathit S, Lee P, Kim CH, Tummala P, Yao W, et al. Osteocytes as mechanosensors in the inhibition of bone resorption due to mechanical loading. Bone. 2008;42(1):172-9.
138. Yokomoto-Umakoshi M, Kanazawa I, Takeno A, Tanaka K-i, Notsu M, Sugimoto T. Activation of AMP-activated protein kinase decreases receptor activator of NF-κB ligand expression and increases sclerostin expression by inhibiting the mevalonate pathway in osteocytic MLO-Y4 cells. Biochemical and biophysical research communications. 2016;469(4):791-6.
139. Wang L, You X, Lotinun S, Zhang L, Wu N, Zou W. Mechanical sensing protein PIEZO1 regulates bone homeostasis via osteoblast-osteoclast crosstalk. Nature Communications. 2020;11(1):282.
140. Sun W, Chi S, Li Y, Ling S, Tan Y, Xu Y, et al. The mechanosensitive Piezo1 channel is required for bone formation. eLife. 2019;8:e47454.
141. Huang J, Romero-Suarez S, Lara N, Mo C, Kaja S, Brotto L, et al. Crosstalk between MLO-Y4 osteocytes and C2C12 muscle cells is mediated by the Wnt/β-catenin pathway. JBMR Plus. 2017;1(2):86-100.
142. Ma J, Zhang ZL, Hu XT, Wang XT, Chen AM. Metformin promotes differentiation of human bone marrow derived mesenchymal stem cells into osteoblast via GSK3β inhibition. Eur Rev Med Pharmacol Sci. 2018;22(22):7962-8.
143. Cheng B, Kato Y, Zhao S, Luo J, Sprague E, Bonewald LF, et al. PGE2 Is Essential for Gap Junction-Mediated Intercellular Communication between Osteocyte-Like MLO-Y4 Cells in Response to Mechanical Strain. Endocrinology. 2001;142(8):3464-73.
144. Liu Q, Yuan W, Tong D, Liu G, Lan W, Zhang D, et al. Metformin represses bladder cancer progression by inhibiting stem cell repopulation via COX2/PGE2/STAT3 axis. Oncotarget. 2016;7(19):28235-46.
145. Tong D, Liu Q, Liu G, Xu J, Lan W, Jiang Y, et al. Metformin inhibits castration-induced EMT in prostate cancer by repressing COX2/PGE2/STAT3 axis. Cancer Lett. 2017;389:23-32.
146. Hyun B, Shin S, Lee A, Lee S, Song Y, Ha N-J, et al. Metformin Down-regulates TNF-α Secretion via Suppression of Scavenger Receptors in Macrophages. Immune Netw. 2013;13(4):123-32.
147. Nasjonalt handlingsprogram med retningslinjer for diagnostikk, behandling og oppfølging av kreft i tykktarm og endetarm: Helsedirektoratet; 2019 [Available from: https://helsedirektoratet.no/retningslinjer/nasjonalt-handlingsprogram-med-retningslinjer-for-diagnostikk-behandling-og-oppfolging-av-kreft-i-tykktarm-og-endetarm.

148. Mortezaee K, Shabeeb D, Musa AE, Najafi M, Farhood B. Metformin as a Radiation Modifier; Implications to Normal Tissue Protection and Tumor Sensitization. Curr Clin Pharmacol. 2019;14(1):41-53.
149. Cheki M, Shirazi A, Mahmoudzadeh A, Bazzaz JT, Hosseinimehr SJ. The radioprotective effect of metformin against cytotoxicity and genotoxicity induced by ionizing radiation in cultured human blood lymphocytes. Mutat Res. 2016;809:24-32.
150. Najafi M, Cheki M, Rezapoor S, Geraily G, Motevaseli E, Carnovale C, et al. Metformin: Prevention of genomic instability and cancer: A review. Mutation Research/Genetic Toxicology and Environmental Mutagenesis. 2018;827:1-8.

Appendix

Appendix 1 : Extract from LDH activity cytotoxicity detection protocol (Roche)

Appendix 2 : RNeasy Mini Kit protocol (p.25-28) (Qiagen)

Appendix 3 : Extract from PGE2 ELISA kit manufacturers protocol (Cayman Chemicals)

Appendix 4 : Extract from Cell death detection kit manufacturers protocol (Roche)

Appendix 5 : RANKL/OPG ratio individual biological replicates

Appendix 1: **Extract from LDH activity cytotoxicity detection protocol (Roche)**

Preparation of working solutions (page 6):

1. Catalyst (bottle 1): Let the lyophilizate dissolve in 1 mL double distilled water for 10 min, then mix thoroughly.
2. Reaction mixture (for 100 tests of 100 µL/test): Shortly before use, mix 250 µL of reconstituted bottle 1 with 11.25 mL of bottle 2.

Measurement of the cytotoxic potential of soluble substances. Procedure for 96-well plate (page 11-12):

1. To determine LDH activity, add 100 µL reaction mixture (freshly prepared) to each well on the 96-well plate and incubate for 5-10 minutes for high cell numbers or up to 30 minutes for low cell numbers (under 100 cells/well) at 15-25 °C. During this incubation, you should protect the plate from light.
2. Add 50 µL stop solution to each well of the 96-well plate. Shake the plate for 10 seconds.
3. Use an ELISA reader to measure the absorbance of the samples at 490 or 492 nm (depending on the filters available in the reader). The reference wavelength should be more than 600 nm.
4. Calculate the percent cytotoxicity for each sample.

Appendix 2: RNeasy Mini Kit protocol (p.25-28) (Qiagen)

1. Harvest cells according to step 1a or 1b.
    a. Cells grown in suspension: Determine the number of cells. Pellet the appropriate number of cells by centrifuging for 5 min at 300 x g in a centrifuge tube. Carefully remove all supernatant by aspiration, and proceed to step 2.
    b. Cells grown in a monolayer (do not use more than $1x10^7$ cells): Cells can be either lysed directly in the cell-culture vessel (up to 10 cm diameter) or trypsinized and collected as a cell pellet prior to lysis. Cells grown in cell-culture flasks should always be trypsinized. To lyse cells directly: Determine the number of cells. Completely aspirate the cell-culture medium, and proceed immediately to step 2.To trypsinize and collect cells: Determine the number of cells. Aspirate the medium, and wash the cells with PBS. Aspirate the PBS, and add 0.1–0.25% trypsin in PBS. After the cells detach from the dish or flask, add medium (containing serum to inactivate the trypsin), transfer the cells to an RNase-free glass or polypropylene centrifuge tube (not supplied) and centrifuge at 300 x g for 5 min. Completely aspirate the supernatant, and proceed to step 2.
2. Disrupt the cells by adding Buffer RLT. For pelleted cells, loosen the cell pellet thoroughly by flicking the tube. Add the appropriate volume of Buffer RLT (see Appendix table 2.1). Vortex or pipet to mix, and proceed to step 3.

Appendix table 2.1: Volumes of Buffer RLT for lysing pelleted cells

Number of pelleted cells	Volume of Buffer RLT (µL)
$<5 \times 10^6$	350
$5x\ 10^6 – 1 \times 10^7$	600

For direct lysis of cells grown in a monolayer, add the appropriate volume of Buffer RLT (Appendix table 2.2) to the cell-culture dish. Collect the lysate with a rubber policeman. Pipet the lysate into a micro centrifuge tube (not supplied). Vortex or pipet to mix, and ensure that no cell clumps are visible before proceeding to step 3.

Appendix table 2.2: Volumes of Buffer RLT for direct cell lysis.

Dish diameter (cm)	Volume of Buffer RLT (µL)*
<6	350
6-10	600

* Regardless of the cell number, use the buffer volumes indicated to completely cover the surface of the dish.

3. Homogenize the lysate according to step 3a, 3b, or 3c. If processing ≤1 x 105 cells, homogenize by vortexing for 1 min. After homogenization, proceed to step 4.
    a. Pipet the lysate directly into a QIAshredder spin column placed in a 2 ml collection tube, and centrifuge for 2 min at full speed. Proceed to step 4.
    b. Homogenize the lysate for 30 s using a rotor–stator homogenizer. Proceed to step4.
    c. Pass the lysate at least 5 times through a blunt 20-gauge needle (0.9 mm diameter) fitted to an RNase-free syringe. Proceed to step 4.

4. Add 1 volume of 70% ethanol to the homogenized lysate, and mix well by pipetting. Do not centrifuge.
5. Transfer up to 700 µL of the sample, including any precipitate that may have formed, to an RNeasy spin column placed in a 2 ml collection tube (supplied). Close the lid gently, and centrifuge for 15 s at ≥8000 x g (≥10,000 rpm). Discard the flow-through.* Reuse the collection tube in step 6. If the sample volume exceeds 700 µL, centrifuge successive aliquots in the same RNeasy spin column. Discard the flow-through after each centrifugation.*
6. Add 700 µL Buffer RW1 to the RNeasy spin column. Close the lid gently, and centrifuge for 15 s at ≥8000 x g (≥10,000 rpm) to wash the spin column membrane. Discard the flow-through.* Reuse the collection tube in step 7. **Note**: After centrifugation, carefully remove the RNeasy spin column from the collection tube so that the column does not contact the flow-through. Be sure to empty the collection tube completely.
7. Add 500 µL Buffer RPE to the RNeasy spin column. Close the lid gently, and centrifuge for 15 s at ≥8000 x g (≥10,000 rpm) to wash the spin column membrane. Discard the flow-through. Reuse the collection tube in step 8. **Note**: Buffer RPE is supplied as a concentrate. Ensure that ethanol is added to Buffer RPE before use.
8. Add 500 µL Buffer RPE to the RNeasy spin column. Close the lid gently, and centrifuge for 2min at ≥8000 x g (≥10,000 rpm) to wash the spin column membrane. The long centrifugation dries the spin column membrane, ensuring that no ethanol is carried over during RNA elution. Residual ethanol may interfere with downstream reactions. **Note**: After centrifugation, carefully remove the RNeasy spin column from the collection tube so that the column does not contact the flow-through. Otherwise, carryover of ethanol will occur.
9. **Optional**: Place the RNeasy spin column in a new 2 ml collection tube (supplied), and discard the old collection tube with the flow-through. Close the lid gently, and centrifuge at full speed for 1 min. Perform this step to eliminate any possible carryover of Buffer RPE, or if residual flow-through remains on the outside of the RNeasy spin column after step 8.
10. Place the RNeasy spin column in a new 1.5 mL collection tube (supplied). Add 30–50 µL RNase-free water directly to the spin column membrane. Close the lid gently, and centrifuge for 1 min at ≥8000 x g (≥10,000 rpm) to elute the RNA.
11. If the expected RNA yield is >30 µg, repeat step 10 using another 30–50 µL RNase free water, or using the eluate from step 10 (if high RNA concentration is required). Reuse the collection tube from step 10. If using the eluate from step 10, the RNA yield will be 15–30% less than that obtained using a second volume of RNase-free water, but the final RNA concentration will be higher.

Appendix 3: Extract from PGE_2 ELISA kit manufacturers protocol (Cayman Chemicals)

Buffer preparation (p.12):

Wash buffer: 5 mL Wash Buffer concentrate from the kit (Item No. 400062) was diluted to a total of 2L UltraPure water and added 1 mL of Polysorbate 20 with a syringe and needle. Storage at 4 °C for 2 months.

ELISA buffer: One vial ELISA buffer concentrate from the kit (Item No. 400060) was diluted in 90 mL UltraPure water. Storage at 4 °C for 2 months.

Preparation of assay-specific reagents (p.20-21)

Prostaglandin E_2 ELISA standard:

1. Reconstitute the contents of the PGE_2 ELISA Standard (Item No. 414014) with 1.0 mL ELISA buffer. The concentration of this solution will be 100 ng/mL (bulk standard). Stable for up to 4 weeks at 4°C. Note: If assaying culture medium samples that have not been diluted with ELISA buffer, culture medium should be used in place of ELISA buffer for dilution of the standard curve.
2. Obtain eight test tubes and number them #1 to #8. Aliqout 900 µL ELISA buffer to tube #1 and 500 µL to tubes #2-8.Transfer 100 µL of the bulk standard to #1 and mix thoroughly. The concentration of this standard, the first point on the standard curve will be 1 ng/mL (1000 pg/mL). Serially dilute the standard by removing 500 µL from tube #1 and placing in tube #2; mix thoroughly. Next, remove 500 µL from tube #2 nd place into tube #3; mix thoroughly. Repeat this for tubes #4-8 (see figure x).

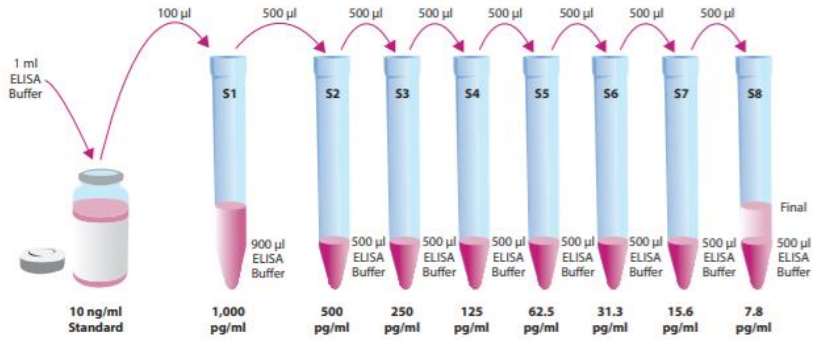

Figure 6. Preparation of the PGE_2 standards

Appendix figure 3.1: Preparation of serial dilution standard curve for PGE_2 ELISA. Figure from manufacturers protocol.

Prostaglandin E_2 AChE tracer: AChE tracer (Item No. 414010) is reconstituted with 6 mL ELISA buffer. Storage at 4 °C for maximum four weeks.

Prostaglandin E_2 Monoclonal antibody: Monoclonal antibody (Item No. 414013) is reconstituted with 6 mL ELISA buffer. Can be stored at 4 °C for at least four weeks.

Performing the assay (p.23-25)

Addition of reagents:

1. ELISA buffer: Add 100 µL ELISA buffer to NSB wells. Add 50 µL ELISA buffer to B_o wells. If culture medium was used to dilute the standard curve, substitute 50 µL of culture medium for ELISA buffer in the NSB and B_o wells.
2. Prostaglandin E_2 ELISA standard: Add 50 µL from tube #8 to both of the lowest standard wells (S8). Add 50 µL from tube #6 to each of the next two standard wells (S7). Continue with this procedure until all standards are aliquoted. The same pipette tip should be used to aliquot all the standards. Before pipetting each standard, be sure to equilibrate the pipette tip in that standard.
3. Samples: Add 50 µL of sample per well. Each sample should be assayed at a minimum of two dilutions. Each dilution should be assayed in duplicate (triplicate recommended).
4. Prostaglandin E_2 AChE tracer: Add 50 µL to each well except the TA and the Blk wells.
5. Prostaglandin E_2 monoclonal antibody: Add 500 µL to each well except the TA, the NSB and the Blk wells.

Appendix table 3.1: Pipetting summary ELISA PGE_2

Well	ELISA buffer	Standard/sample	Tracer	Antibody
Blk	-	-	-	-
TA	-	-	5 µL (at devl.step)	-
NSB	100 µL	-	50 µL	-
B_o	50 µL	-	50 µL	50 µL
Std/sample	-	50 µL	50 µL	50 µL

Incubation of the plate: Cover the plate with plastic film (Item No. 400012) and incubate 18 hours at 4 °C.

Development of the plate:

1. Reconstitute Ellman's reagent immediately before use. Ellman's reagent (Item No. 400050) is reconstituted in 20 mL UltraPure water. Should be protected from light when not in use.
2. Empty the wells and rinse five times with Wash Buffer.
3. Add 200 µL of Ellman's Reagent to each well.
4. Add 5 µL of tracer to TA wells.
5. Cover the plate with plastic film. Optimum development is obtained by using an orbital shaker equipped with a large, flat cover to allow the plate to develop in the dark. This assay typically develops (i.e. B_o wells >0.2 A.U. (blank subtracted)) in 60-90 minutes.

Reading the plate:

1. Wipe the bottom of the plate with a clean tissue to remove fingerprints, dirt etc.
2. Remove the plate cover being careful to keep Ellman's Reagent from splashing on the cover. NOTE: Any loss of Ellman's reagent will affect the absorbance readings. If Ellman's Reagent is present on the cover, use a pipette to transfer the reagent back into the well. If too much Ellman's reagent has splashed on the cover to easily redistribute back into the wells, wash the plate three times with wash buffer and repeat the developemnt with fresh Ellman's reagent.
3. Read the plate at a wavelength between 405 and 420 nm. The absorbance may be checked periodiaclly until the B_o wells have reached a minimum of 0.3 A.U (blank subtracted). The plate should be read when the absorbance of the B_o are in the range of 0.3-1.0 A.U (blank subtracted). If the absorbance of the wells exceeds 1.5, wash the plate, add fresh Ellman's reagent and let it develop again.

Appendix 4: Extract from Cell death detection kit manufacturers protocol (Roche)

Preparation of working solutions:

1. Anti-histone biotine, anti-DNA POD and positive control: Reconstitute the lyophilizate in 450 µL double distilled water for 10 minutes and mix thourougly. Stable for two months at 4 °C.
2. Incubation buffer, lysis buffer and ABTS Stop solution is ready-to-use. Stable at 4 °C until expiration date.
3. ABTS substrate: Dependent on the number of samples tested, dissolve 1, 2 or 3 ABTS tablets in 5, 10 or 15 mL substrate buffer. Store protected from light for one month at 4 °C.

Preparation of immunoreagent: Prepare the solution shorthly before use as shown in Appendix table 4.1, and do not store. Homogenize thoroughly.

Appendix table 4.1: Preparation of immunoreagent for cell death detection ELISA kit.

# of tests	**100**
Incubation buffer	7.2 mL
Anti-histone-biotine	0.4 mL
Anti-DNA-POD	0.4 mL
Immunoreagent total amount	8 mL

Sample preparation:

1. Centrifuge the microplate for 10 minutes, with 200 x g.
2. If you do not want to analyze necrosis, remove the supernatant carefully.
3. Resuspend the cell pellet in 200 µL 1x working solution of Lysis buffer. Incubate for 30 minutes at room temperature (cell lysis). Adherent cells can be lysed directly in the well without prior removal.
4. Centrifuge the lysate at 200 x g for 10 minutes.
5. Transfer 20 µL of the supernatant carefully into the streptavidin coated microplate for analysis (do not shake the pellet). Samples should be analyzed immediately.

ELISA assay:

1. Transfer 20 µL from lysates of treated cells after centrifugation, positive control, negative control (untreated cells) and background control (incubation buffer) into the microplate.
2. Add to each well 80 µL of the immunoreagent.
3. Cover the microplate with an adhesive cover foil and incubate on a microplate shaker under gently shaking (300 rpm) for 2 hours at room temperature.
4. Rinse the solution thoroughly by tapping. Rinse each well 3x with 250-300 µL incubation buffer and remove solution carefully.

5. Pipette to each well 100 µL ABTS substrate solution and incubate on a plate shaker at 250 rpm until the color development is sufficient for a photometric analysis (approx. after 10-20 minutes).
6. Pipette to each well 100 µL ABTS stop solution.
7. Measure at 405 nm against ABTS substrate solution + 100 µL ABTS stop solution as a blank. Reference wavelength approx. 490 nm.

Appendix 5: RANKL/OPG ratio individual biological replicates

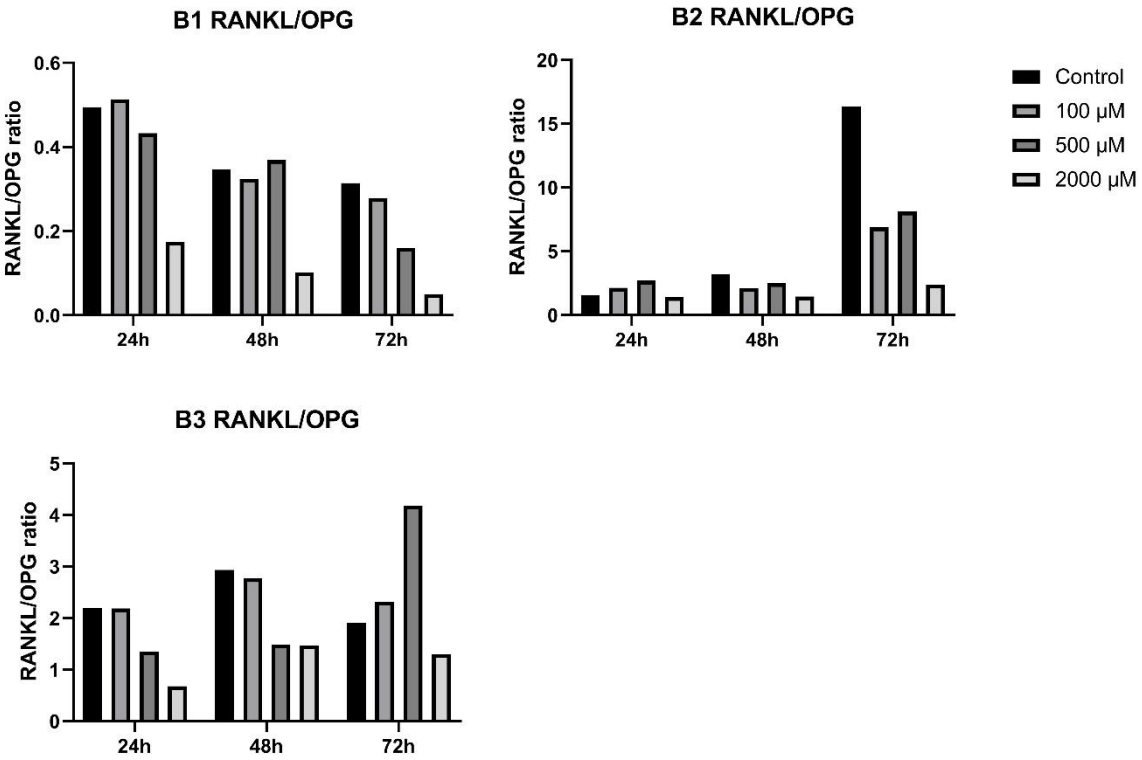

Appendix figure 5.1: RANKL/OPG ratio mRNA expression. Each biological replicate is shown in individual graph (B1, B2 and B3). The reported values are means of RANKL divided by means of OPG within one biological replicate.

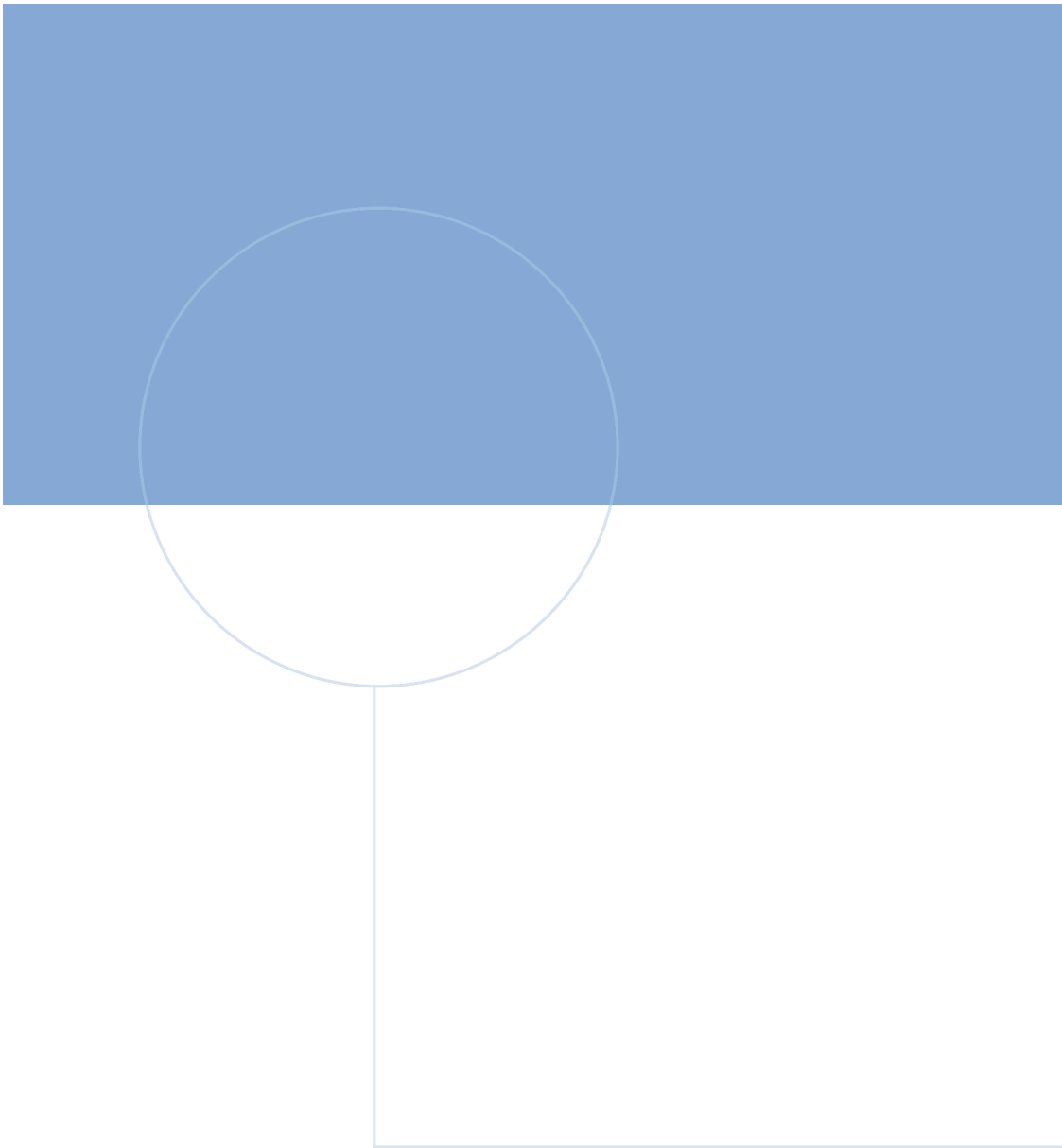

NTNU

Norwegian University of
Science and Technology